Available online at www.sciencedirect.com
ScienceDirect
Comput. Methods Appl. Mech. Engrg. 197 (2008) 623–640
Computer methods in applied mechanics and engineering
www.elsevier.com/locate/cma

A formulation based on localized Lagrange multipliers for BEM–FEM coupling in contact problems

José A. González [a,*], K.C. Park [b], Carlos A. Felippa [b], Ramón Abascal [a]

[a] *Escuela Superior de Ingenieros de Sevilla, Camino de los Descubrimientos s/n, 41092 Seville, Spain*
[b] *Department of Aerospace Engineering Sciences, Center for Aerospace Structures, University of Colorado, Boulder, CO 80309-0429, USA*

Received 7 February 2007; received in revised form 18 July 2007; accepted 19 August 2007
Available online 14 September 2007

Abstract

This paper presents a unified formulation for the combination of the finite element method (FEM) and the boundary element method (BEM) in 3D frictional contact problems that is based on the use of localized Lagrange multipliers (LLMs). Resolution methods for the contact problem between non-matching meshes have traditionally been based on a direct coupling of the contacting solids using classical Lagrange multipliers. These methods tend to generate strongly coupled systems that require a deep knowledge of the discretization characteristics on each side of the contact zone complicating the process of mixing different numerical techniques. In this work a displacement *contact frame* is inserted between the FE and BE interface meshes, discretized and finally connected to the contacting substructures using LLMs collocated at the mesh-interface nodes. This methodology will provide a partitioned formulation which preserves software modularity and facilitates the connection of non-matching FE and BE meshes.
© 2007 Elsevier B.V. All rights reserved.

Keywords: Contact; Finite element method; Boundary element method; Localized Lagrange multipliers

1. Introduction

In computational structural mechanics, problems involving frictional contact surfaces combined with non-matching meshes are often considered a difficult task even when using the same numerical method for the two substructures participating in the contact process. The source of this difficulty comes not only from the strong non-linearity of the frictional contact law, involving multi-valued relationships between kinematic and static variables, but also from the severe discontinuity forced by the different meshes used to model the contact interface. Such a difficulty explains the existence of many alternatives to treat the problem, differing for example in the way that the contact conditions are imposed: exactly, approximately or in a weak-form, with differences in the range of applications considered: conformal contact, frictionless, with friction, or in the approach used to treat the contact process: node to node, node to element or node to surface.

Two of the best known techniques to solve the contact problem are the penalty method and the Lagrange multiplier method. In the penalty method the displacement constraints are imposed in an approximated way introducing some extra stiffness terms in the global stiffness matrix to force the numerical fulfilment of the contact conditions with a predefined degree of error. This approach usually uses contact elements to control the gap and relative tangential displacements between the nodes of a master substructure and the elements of a contacting slave substructure. The main disadvantage of this method is that the resulting system of equations often suffers from ill-conditioning due to important differences between the natural structural stiffness and the artificial stiffness terms introduced to impose the contact conditions.

A preferred alternative is the Lagrange multiplier method that was first introduced by Hughes et al. [18] for contact-impact problems. This method is based on

* Corresponding author.
E-mail address: japerez@us.es (J.A. González).

0045-7825/$ - see front matter © 2007 Elsevier B.V. All rights reserved.
doi:10.1016/j.cma.2007.08.020

introducing a new set of unknowns into the equations of motion representing the interface contact forces and has evolved from its initial formulation, restricted to frictionless node to node contact situations, to more recent proposals adopting node to element master–slave approaches with dissimilar meshes.

However and related with the solution of contact problems interfacing non-matching meshes, classical node to element techniques showed their incapacity of passing the contact patch tests proposed by Taylor and Papadopoulos [32] and Crisfield [6]. Faced with this and other shortcomings of classical node to surface approaches, some researches like Simó et al. [31] and Papadopoulos and Taylor [23] proposed the idea of introducing an intermediate contact surface, an explicit representation of the contact zone, where contact variables could be defined and interpolated. A more complete overview of the different approaches used in FE contact problems can be found in the books of Wriggers [34] and Laursen [19].

In recent years, techniques and approximations initially designed for domain decomposition problems with non-matching meshes are being applied to contact mechanics; examples of these techniques are the mortar method and the LLM method.

In the mortar method two different discretized surfaces are connected using Lagrange multipliers; these multipliers are approximated by shape functions which have to match the displacement approximation in order to arrive at a stable discretization scheme. The first extension of the mortar FEM to the unilateral contact problem was made by Belgacem et al. [3] presenting a theoretical basis that was implemented by Hild [16]. Later different proposals arrived; for example the work of McDevitt and Laursen [20] using the mortar method to variationally project displacements from contacting continua to an intermediate surface, more recently its application to segment contact by Puso and Laursen [28], the work of Fisher et al. [9] solving frictionless large deformation contact problems using non-matching meshes and mortar methods, and the dual mortar method proposed by Wohlmuth [33] applied to 2D contact problems in elasticity by Flemish et al. [10].

The LLM method proposed by Park and Felippa [24–26] is a general variational framework used to solve partitioned systems in structural mechanics that also introduces between the substructures an intermediate surface called *frame*, that is endowed with independent degrees of freedom and treated with a FEM discretization to approximate the interface variables. Finally, this *frame* is connected to the substructures using classical Lagrange multipliers defined on the substructure interface nodes, obtaining an approximation that naturally allows the treatment of non-matching meshes and can be constructed in order to preserve the constant-stress interface patch test, as demonstrated by Park et al. [27].

This localized approach, initially dedicated to structural substructuring and coupled problems, was later extended to contact problems by Rebel et al. [29] who treated the two dimensional frictional contact problem between non-matching meshes using an intermediate contact surface that was named *contact frame*. However, Rebel et al. considered the contact zone to be a priori known after applying a two stages predictor–corrector algorithm to find the *contact frame* position and decided the contact point states using a *trial and error* based algorithm that was revisited after each contact iteration. Later, González et al. [13] allowed the *contact frame* to separate from the substructures in all directions, making the frame a completely free system between the substructures that moves maintaining the contact zone as an unknown. Differences in this work were also in the way of finding the contact states, because the contact conditions were imposed mathematically using an augmented Lagrangian formulation with projection functions, making the *trial and error* contact search unnecessary.

In contact problems the region of interest is usually restricted to a local area around the contact zone where stress concentration with locally plastic deformations can occur, while extensive parts of the solid remain almost unloaded. This is a situation well suited for a combination of the FEM and the BEM, but the main difficulty when mixing locally or inside a particular substructure the FEM and the BEM is that the system of equations produced by these two methods are expressed in different variables and cannot be linked without modifications. Many coupling techniques have been proposed trying to alter the formulation of one of the methods to make it compatible with the other combining their advantages. The first BEM–FEM coupling formulations were proposed in the pioneering works of Zienkiewicz et al. [35,36] and Brebbia and Georgiou [4] that formulated the problem using two different points of view; the first one considers the BE region as a FE region, forcing a symmetrization of the BE substructure on the basis of energy error minimization considerations; and the second one tries to reformulate the FE region to make it compatible with the BE equations. In this area, González et al. [14] proposed a novel method to couple the FEM and the BEM using LLMs and the variational framework developed by Park and Felippa, introducing the BEM elastic equations with the boundary tractions transformed into forces and connecting them to a *frame* where the interface displacements were interpolated.

Most of the contributions mixing the BEM and the FEM in contact problems do not consider a change of the numerical method through the contact interface, combining these numerical methods only inside the contacting substructures and assuming at the end a FEM–FEM or BEM–BEM contact approach. Examples are the works of Ezawa and Okamoto [8] using special contact elements and Oysu and Fenner [21] coupling the BEM and the FEM locally in elastoplastic contact problems.

In this work we extend the contact formulation using LLMs of [13] with the BEM–FEM coupling technique proposed in [14], demonstrating the modularity and

extensibility of partitioned approximations based on LLMs. The resulting formulation will be applied to the solution of 3D frictional contact problems between the FEM and the BEM with non-matching meshes.

2. Notation

The notation of the expressions contained in this paper is based on the following conventions: vectors and tensors are written in bold-face, repeated tensor and matrix indices appearing as both sub/super-index imply summation and repeated indices that appear only as subindex do *not* imply summation. Also the usual convention that Greek indices run from 1 to 2 will be adopted.

3. Contact frame

Let us consider two solids in contact and denote their domains Ω and $\overline{\Omega}$ with a common interface Γ_c. To formulate the contact problem, instead of considering the direct interaction between these two bodies during the contact process, we will insert a deforming non-physical surface called *contact frame* Λ with $\Gamma_c \subset \Lambda$ and reformulate the contact problem in terms of interaction of the solids with this auxiliary surface using LLMs collocated on each side of the frame.

The contact forces acting on the frame are represented in the exploded view of Fig. 1 where the LLMs connecting the solid Ω with the frame are named using the vector quantity $\boldsymbol{\lambda} = (\lambda_n, \lambda_t^1, \lambda_t^2)^t$ and the multipliers connecting solid $\overline{\Omega}$ are named $\bar{\boldsymbol{\lambda}} = (\bar{\lambda}_n, \bar{\lambda}_t^1, \bar{\lambda}_t^2)^t$. These forces are expressed using two locally orthonormal base systems attached to the frame; $\mathbf{B} = [\mathbf{n}, \mathbf{a}_1, \mathbf{a}_2]$ used to describe $\boldsymbol{\lambda}$ and $\overline{\mathbf{B}} = [\bar{\mathbf{n}}, \bar{\mathbf{a}}_1, \bar{\mathbf{a}}_2]$ used for $\bar{\boldsymbol{\lambda}}$. These frame local systems are defined in the following way; $\mathbf{a}_1$ and $\mathbf{a}_2$ are the orthogonal vectors contained in the frame tangent plane at the considered point and vector $\mathbf{n}$ points towards solid $\overline{\Omega}$. The barred base system $\overline{\mathbf{B}}$ at the same position, will be defined in opposite direction to $\mathbf{B}$.

A key approach of the present localized formulation is to treat the non-matching contact interfaces by the method of LLMs using either the BEM or the FEM to model the contacting solids.

3.1. Frame kinematics

In order to describe the motion of the two solids we use the displacement fields $\mathbf{u}$ and $\bar{\mathbf{u}}$ defined on Ω and $\overline{\Omega}$, respectively, see Fig. 2, that added to the reference configurations $\mathbf{X}$ and $\overline{\mathbf{X}}$ provides us with the current positions $\mathbf{x}$ and $\bar{\mathbf{x}}$

$$\begin{aligned} \mathbf{x} &= \mathbf{X} + \mathbf{u}, \\ \bar{\mathbf{x}} &= \overline{\mathbf{X}} + \bar{\mathbf{u}} \end{aligned} \tag{1}$$

magnitudes expressed in the global system.

The motion of the contact frame is described using its displacements $\mathbf{v}$ from its initial configuration $\mathbf{Y}$, providing a current position

$$\mathbf{y} = \mathbf{Y} + \mathbf{v}, \tag{2}$$

however, this motion will be restricted to permanently maintain the frame just in the middle between the solids. To do that, the relative frame–solid distance vectors $\mathbf{k} = (k_n, k_t^1, k_t^2)^t$ and $\bar{\mathbf{k}} = (\bar{k}_n, \bar{k}_t^1, \bar{k}_t^2)^t$ are expressed in the frame local system by

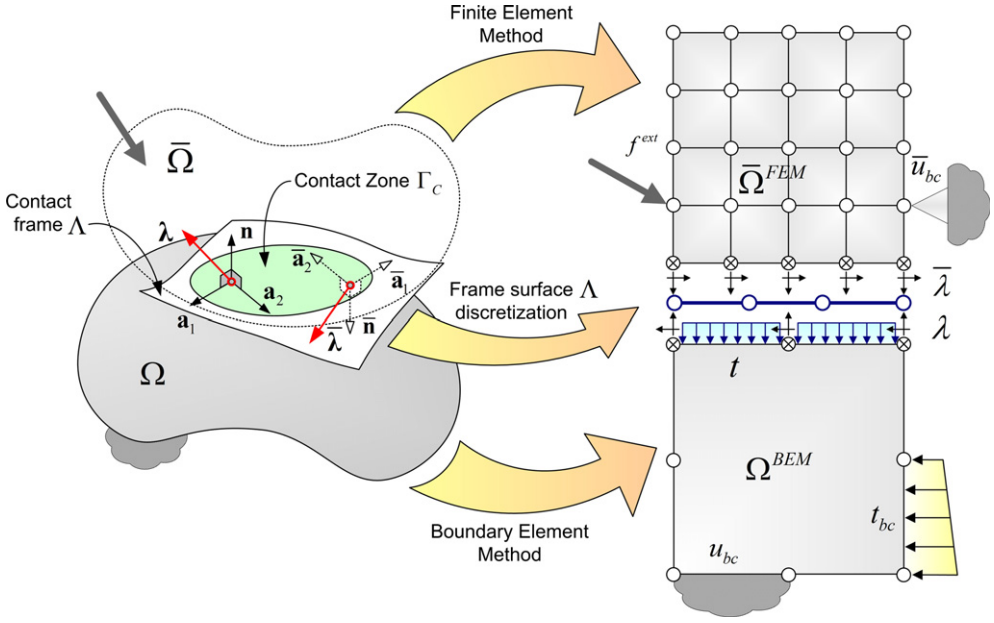

Fig. 1. Left: Abstract representation of two solids in contact with an intercalated frame. Right: Discrete approximation with localized Lagrange multipliers connecting the BE and FE meshes to the frame.

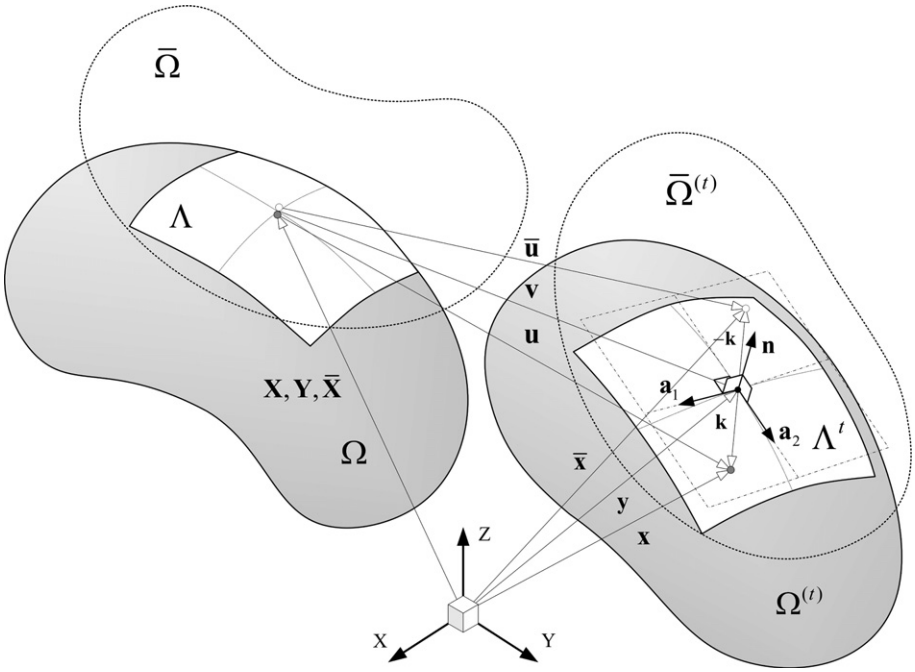

Fig. 2. Kinematic description of the relative motion between two substructures with a contact frame situated between them. The symbol ● is used to describe the motion of a boundary particle from solid Ω and ○ for a particle from solid $\bar{\Omega}$.

$$\begin{aligned} k_n &= \mathbf{n}\cdot(\mathbf{x}-\mathbf{y}), \quad \bar{k}_n = \bar{\mathbf{n}}\cdot(\bar{\mathbf{x}}-\mathbf{y}),\\ k_t^1 &= \mathbf{a}_1\cdot(\mathbf{x}-\mathbf{y}), \quad \bar{k}_t^1 = \bar{\mathbf{a}}_1\cdot(\bar{\mathbf{x}}-\mathbf{y}),\\ k_t^2 &= \mathbf{a}_2\cdot(\mathbf{x}-\mathbf{y}), \quad \bar{k}_t^2 = \bar{\mathbf{a}}_2\cdot(\bar{\mathbf{x}}-\mathbf{y}) \end{aligned} \tag{3}$$

or more compactly

$$\begin{aligned} \mathbf{k} &= \mathbf{B}^{\mathbf{t}}(\mathbf{x}-\mathbf{y}),\\ \bar{\mathbf{k}} &= \overline{\mathbf{B}}^{\mathbf{t}}(\bar{\mathbf{x}}-\mathbf{y}) \end{aligned} \tag{4}$$

and forced to be the same on each side of the frame, i.e. $\mathbf{k}=\bar{\mathbf{k}}$.

With previous definitions the contact frame matches with the contact zone Γ_c where k_n is equal to zero. Also $\mathbf{k}_t=(k_t^1,k_t^2)^t$ will give us the direction of the relative motion of the solids in the interface, a variable needed to formulate the frictional behavior.

We choose the reference position of the frame $\mathbf{Y}$ to be the *current* position of the contact frame. This is done in order to define $\mathbf{k}_t$ as the tangential slip increment and allows to change the geometry of the frame during the contact process.

4. Enforcement of the contact conditions

The behavior at the contact interface is governed by the non-penetration condition in the normal direction to the contact zone and the frictional tribological law in the tangential direction. The tribological model used in this work is the Coulomb friction law, a common engineering approximation to the frictional process where normal and tangential tractions are coupled by the normal pressure.

When applying the contact conditions, one difficulty reside in the fact that contact restrictions are given by a group of equalities and inequalities resulting in a constrained optimization problem. To avoid this complication we use the augmented Lagrangian formulation of the frictional contact problem proposed by Alart and Curnier [2], Simó and Laursen [30] and De Saxce and Feng [7]; based on reformulating the unilateral contact law and the frictional law as a system of equations without inequalities. This method solves the contact problem exactly in contrast to other penalty formulations, however, the equation system obtained is non-differentiable but B-differentiable as pointed out by Christensen et al. [5], and therefore, the classical Newton method for smooth equations fails to be applicable.

4.1. Normal direction: unilateral contact law

In the normal direction, the contact problem is governed by the non-penetration condition. This kinematic condition imposes that the *gap* between the contacting surfaces must remain always positive (then we say there is a *separation* situation) or zero (corresponding to a *contact* situation). Instead of using the *gap* variable to formulate the normal contact we will use the *normal penetration* k_n, the same variable but with its sign changed. To quantify the normal penetration, we calculate the relative vector between two particles and project it on the contact frame normal

$$k_n = (\mathbf{x}-\mathbf{y})\cdot\mathbf{n} \tag{5}$$

magnitude that must remain always negative in separation, or equal to zero in contact.

The penetration variable possesses a complementarity relation with its counterpart, the surface normal force λ_n. When there is a separation ($k_n < 0$) the normal force is zero ($\lambda_n = 0$) and only when there is a contact ($k_n = 0$) we can have a reaction ($\lambda_n \geqslant 0$). This behavior can be mathematically expressed by the complementarity condition

$$\begin{cases} \lambda_n k_n = 0, \\ \lambda_n \geqslant 0, k_n \leqslant 0 \end{cases} \tag{6}$$

composed by two inequalities.

Previous inequalities can be eliminated expressing Eq. (6) using projection functions. Let us define the projection function on the real positive line $\mathbb{P}_{\mathbb{R}^+}(.) : \mathbb{R} \to \mathbb{R}$ in the following way:

$$\mathbb{P}_{\mathbb{R}^+}(x) = \max(0, x) \tag{7}$$

and define the *augmented normal variable* $\lambda_n(r)$ as

$$\lambda_n(r) = \lambda_n + r k_n, \tag{8}$$

where $r > 0$ is a penalty parameter. Then conditions (6) can be expressed using only one equation

$$\mathbb{P}_{\mathbb{R}^+}(\lambda_n(r)) = \lambda_n \tag{9}$$

that guaranties by itself the fulfilment of unilateral contact conditions. However, the price we have to pay for this simplification is that (9) is no longer a strictly differentiable function because there is one point where only the directional derivative can be computed, exactly in the frontier between *contact* and *separation*.

4.2. Tangential direction: Coulomb friction law with variable pressure

The tangential motion of the contact frame is governed by the frictional behavior; this behavior imposes that when there is *contact* between two boundary particles, they will remain together in *stick* condition if their tangential stresses do not reach a *friction limit* g. If that friction limit is reached, the tangential stress will remain constant during a *slip* in the same direction of the surfaces relative motion.

Special care is needed when imposing the frictional contact condition with the sign of the frictional work; this frictional work must be negative in order to represent a dissipative system, condition satisfied by sign criteria represented in Fig. 3.

The Coulomb friction law establishes that if we define the *Coulomb disk* of radius g as

$$\mathbb{C}_g(x, y) = \{(x, y) \in \mathbb{R}^2 : x^2 + y^2 \leqslant g^2\}$$

the tangential conditions can be written

$$\boldsymbol{\lambda}_t \in \mathbb{C}_g \quad \text{and} \quad \mathbf{k}_t = \begin{cases} \mathbf{0} & \text{if } \|\boldsymbol{\lambda}_t\| < g, \\ \gamma \boldsymbol{\lambda}_t \text{ with } \gamma \geqslant 0 & \text{if } \|\boldsymbol{\lambda}_t\| = g \end{cases} \tag{10}$$

with $\gamma \in \mathbb{R}^+$ to make sure that the tangential slip increment $\mathbf{k}_t$ and the tangential force $\boldsymbol{\lambda}_t = (\lambda_t^1, \lambda_t^2)^t$ have the same sign and our system is dissipative.

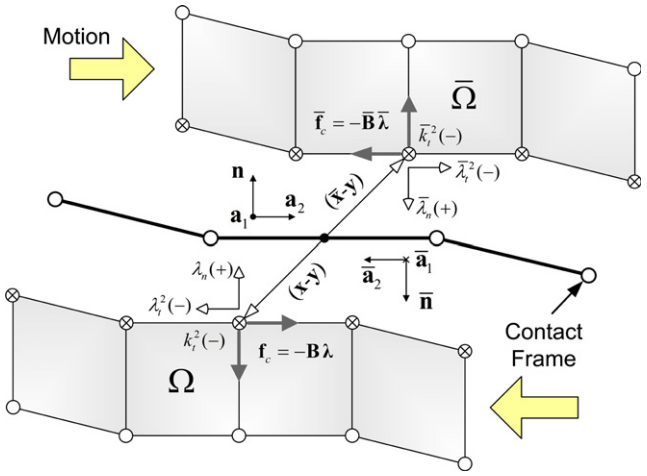

Fig. 3. Exploded view with sign criteria used for the Lagrange multipliers and contact forces in a FEM–FEM contact zone. A relative motion of the two substructures in the indicated direction will produce represented signs on contact forces.

Previous conditions can also be reduced to the fulfilment of only one equation; to do that, we define the Coulomb disk projection operator $\mathbb{P}_{\mathbb{C}_g}(.) : \mathbb{R}^2 \to \mathbb{R}^2$ in the following way:

$$\mathbb{P}_{\mathbb{C}_g}(x, y) = \begin{cases} [x, y]^t & \text{if } x^2 + y^2 \leqslant g^2, \\ \frac{g}{\sqrt{x^2+y^2}}[x, y]^t & \text{otherwise} \end{cases} \tag{11}$$

and introduce the *augmented tangential multiplier* variable

$$\boldsymbol{\lambda}_t(r) = \boldsymbol{\lambda}_t + r\mathbf{k}_t \tag{12}$$

so conditions (10) can be expressed projecting this augmented tangential variable on the disk of radius g, i.e.

$$\mathbb{P}_{\mathbb{C}_g}(\boldsymbol{\lambda}_t(r)) = \boldsymbol{\lambda}_t \tag{13}$$

obtaining again a strictly non-differentiable function at the *stick–slip* frontier but with computable directional derivative at that point.

4.3. Coupled contact conditions

The complete fulfilment of contact conditions comes from a combination of Eqs. (9) and (13), coupled by the fact that the *friction limit* is a function of the normal traction; in the particular case of the Coulomb friction law $g = \mu\lambda_n$ where μ is the *friction coefficient*.

To consider that normal Lagrange multiplier λ_n can only be positive, we make $g = \mu \max(0, \lambda_n)$ and define the cone projection operator $\mathbb{P}_{\triangleleft}(.) : \mathbb{R}^3 \to \mathbb{R}^3$ applied to the augmented Lagrangian multiplier $\boldsymbol{\lambda}(r) = \boldsymbol{\lambda} + r\mathbf{k}$ in the following way:

$$\mathbb{P}_{\triangleleft}(\boldsymbol{\lambda}(r)) = \begin{bmatrix} \mathbb{P}_{\mathbb{R}^+}(\lambda_n(r)) \\ \mathbb{P}_{\mathbb{C}_{\mu\max(0,\lambda_n)}}(\boldsymbol{\lambda}_t(r)) \end{bmatrix}. \tag{14}$$

This definition allows us to express the contact conditions with the final expression

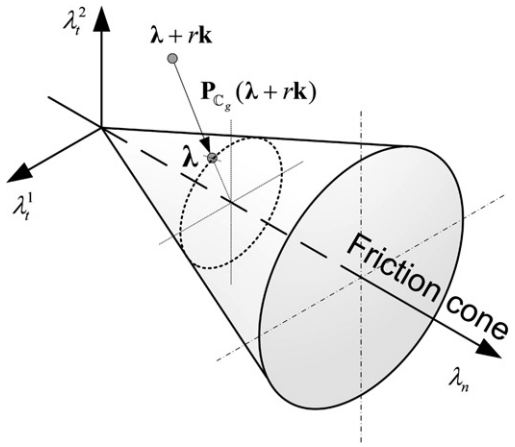

Fig. 4. The projection operator is applied to the augmented variable $\boldsymbol{\lambda}+r\mathbf{k}$. If the contact conditions are fulfiled, the projection operation will return the Lagrangian multipliers back.

$$\mathbb{P}_{\triangleleft}(\boldsymbol{\lambda}(r))=\boldsymbol{\lambda}. \tag{15}$$

The idea behind the cone projection operator (14) is represented in Fig. 4; the contact conditions will be satisfied when a projection of the augmented Lagrange multipliers on the friction cone returns the multipliers back.

5. Variational formulation

To derive the equilibrium equations of the constrained system we use the variational formulation proposed by Park and Felippa [24,25] where the problem is treated like if all bodies were entirely free, formulating the virtual work of the system by summing up the contributions of each body and adding the interface contribution obtained when multiplying the constraint equations by the LLMs.

The variational functional that represents the total energy of the system $\delta\Pi$ is then composed by the energy of the two substructures plus the interface constraint functional associated with the contact phenomena

$$\delta\Pi=\delta\pi^{\text{body }1}+\delta\bar{\pi}^{\text{body }2}+\delta\pi^{\text{int}}, \tag{16}$$

where the contact interface potential $\delta\pi^{\text{int}}$ groups contributions from both sides

$$\delta\pi^{\text{int}}=\delta\pi_i+\delta\bar{\pi}_i \tag{17}$$

and will be derived in this section.

To do that, let us decompose each one of the two interface functionals into two terms

$$\begin{aligned}\delta\pi_i&=\delta\pi_k+\delta\pi_c,\\ \delta\bar{\pi}_i&=\delta\bar{\pi}_k+\delta\bar{\pi}_c\end{aligned} \tag{18}$$

the first one is related with the kinematic positioning of the frame, Eq. (4), that is enforced in a weak sense using the variational form

$$\delta\pi_k=\int\int_{\Gamma_c}(\delta\{\boldsymbol{\lambda}\cdot[\mathbf{B}^{\mathbf{t}}(\mathbf{x}-\mathbf{y})-\mathbf{k}]\})\mathrm{d}\Gamma_c \tag{19}$$

and the second one represents the virtual work of the contact forces, contribution to the weak form that can be expressed in the following way:

$$\delta\pi_c=\int\int_{\Gamma_c}(\boldsymbol{\lambda}\cdot\delta\mathbf{k})\mathrm{d}\Gamma_c, \tag{20}$$

where the contact forces $\boldsymbol{\lambda}$ have to satisfy the unilateral contact law (6) and the frictional law (10). These restrictions can be automatically satisfied replacing the Lagrange multipliers by the projection operator (14) obtaining

$$\delta\pi_c=\int\int_{\Gamma_c}(\mathbb{P}_{\triangleleft}(\boldsymbol{\lambda}(r))\cdot\delta\mathbf{k})\mathrm{d}\Gamma_c \tag{21}$$

equation that added to (19) and substituted back in (18) provides the expression for the total variation of the interface potential at the non-barred side

$$\begin{aligned}\delta\pi_i=\int\int_{\Gamma_c}&(\boldsymbol{\lambda}\cdot\delta\{\mathbf{B}^{\mathbf{t}}(\mathbf{x}-\mathbf{y})\}+\delta\boldsymbol{\lambda}\cdot\{\mathbf{B}^{\mathbf{t}}(\mathbf{x}-\mathbf{y})-\mathbf{k}\}\\&+\delta\mathbf{k}\cdot\{-\boldsymbol{\lambda}+\mathbb{P}_{\triangleleft}(\boldsymbol{\lambda}(r))\})\mathrm{d}\Gamma_c\end{aligned} \tag{22}$$

and similarly

$$\begin{aligned}\delta\bar{\pi}_i=\int\int_{\Gamma_c}&(\bar{\boldsymbol{\lambda}}\cdot\delta\{\overline{\mathbf{B}}^{\mathbf{t}}(\bar{\mathbf{x}}-\mathbf{y})\}+\delta\bar{\boldsymbol{\lambda}}\cdot\{\overline{\mathbf{B}}^{\mathbf{t}}(\bar{\mathbf{x}}-\mathbf{y})-\mathbf{k}\}\\&+\delta\mathbf{k}\cdot\{-\bar{\boldsymbol{\lambda}}+\mathbb{P}_{\triangleleft}(\bar{\boldsymbol{\lambda}}(r))\})\mathrm{d}\Gamma_c\end{aligned} \tag{23}$$

for the barred side.

To deal with the first term of Eqs. (22) and (23) we decompose them in the following way:

$$\begin{aligned}\boldsymbol{\lambda}\cdot\delta\{\mathbf{B}^{\mathbf{t}}(\mathbf{x}-\mathbf{y})\}&=(\delta\mathbf{u}-\delta\mathbf{v})\cdot\{\mathbf{B}\lambda\}+\lambda_n\delta\mathbf{n}\cdot(\mathbf{x}-\mathbf{y})\\&\quad+\lambda_t^{\alpha}\delta\mathbf{a}_{\alpha}\cdot(\mathbf{x}-\mathbf{y}),\end{aligned} \tag{24}$$

$$\begin{aligned}\bar{\boldsymbol{\lambda}}\cdot\delta\{\overline{\mathbf{B}}^{\mathbf{t}}(\bar{\mathbf{x}}-\mathbf{y})\}&=(\delta\bar{\mathbf{u}}-\delta\mathbf{v})\cdot\{\overline{\mathbf{B}}\bar{\lambda}\}+\bar{\lambda}_n\delta\bar{\mathbf{n}}\cdot(\bar{\mathbf{x}}-\mathbf{y})\\&\quad+\bar{\lambda}_t^{\alpha}\delta\bar{\mathbf{a}}_{\alpha}\cdot(\bar{\mathbf{x}}-\mathbf{y})\end{aligned} \tag{25}$$

and considering that if the base system $\mathbf{a}_{\alpha}$ is orthonormal, the variation of the normal and tangential frame unitary vectors can be written (see [37])

$$\delta\mathbf{a}_{\alpha}=\mathbf{Q}_{\alpha}\delta\mathbf{v}_{,\alpha},\quad \delta\bar{\mathbf{a}}_{\alpha}=\overline{\mathbf{Q}}_{\alpha}\delta\mathbf{v}_{,\alpha}, \tag{26}$$

$$\delta\mathbf{n}=\mathrm{e}^{\beta\alpha}(\mathbf{a}_{\beta}\times\mathbf{I})\mathbf{Q}_{\alpha}\delta\mathbf{v}_{,\alpha},\quad \delta\bar{\mathbf{n}}=\mathrm{e}^{\beta\alpha}(\bar{\mathbf{a}}_{\beta}\times\mathbf{I})\overline{\mathbf{Q}}_{\alpha}\delta\mathbf{v}_{,\alpha}, \tag{27}$$

where $\mathbf{Q}_{\alpha}=\frac{1}{\|\mathbf{y}_{,\alpha}\|}(\mathbf{I}-\mathbf{a}_{\alpha}\otimes\mathbf{a}_{\alpha})$, $\overline{\mathbf{Q}}_{\alpha}=\frac{1}{\|\mathbf{y}_{,\alpha}\|}(\mathbf{I}-\bar{\mathbf{a}}_{\alpha}\otimes\bar{\mathbf{a}}_{\alpha})$ and $\mathrm{e}^{\beta\alpha}$ represents the permutation symbol, substitution into (22) and (23) leads to the final expression for the interface potentials

$$\begin{aligned}\delta\pi_i=\int\int_{\Gamma_c}&(\delta\boldsymbol{\lambda}\cdot\{\mathbf{B}^{\mathbf{t}}(\mathbf{x}-\mathbf{y})-\mathbf{k}\}+(\delta\mathbf{u}-\delta\mathbf{v})\cdot\{\mathbf{B}\boldsymbol{\lambda}\}\\&+\delta\mathbf{v}_{,\alpha}\cdot\{\mathbf{Q}_{\alpha}\boldsymbol{\Phi}^{\alpha}(\mathbf{x}-\mathbf{y})\}+\delta\mathbf{k}\cdot\{-\boldsymbol{\lambda}+\mathbb{P}_{\triangleleft}(\boldsymbol{\lambda}(r))\})\mathrm{d}\Gamma_c\end{aligned} \tag{28}$$

with $\boldsymbol{\Phi}^{\alpha}=\lambda_t^{\alpha}\mathbf{I}+\lambda_n\mathrm{e}^{\alpha\beta}(\mathbf{a}_{\beta}\times\mathbf{I})$ and for the barred side

$$\delta\bar{\pi}_i = \int\int_{\Gamma_c} (\delta\bar{\boldsymbol{\lambda}} \cdot \{\overline{\mathbf{B}}^{\mathbf{t}}(\bar{\mathbf{x}} - \mathbf{y}) - \mathbf{k}\} + (\delta\bar{\mathbf{u}} - \delta\mathbf{v}) \cdot \{\overline{\mathbf{B}\bar{\boldsymbol{\lambda}}}\} + \delta\mathbf{v}_{,\alpha} \cdot \{\overline{\mathbf{Q}}_\alpha \bar{\boldsymbol{\Phi}}^\alpha(\bar{\mathbf{x}} - \mathbf{y})\} + \delta\mathbf{k} \cdot \{-\bar{\boldsymbol{\lambda}} + \mathbb{P}_{\lhd}(\bar{\boldsymbol{\lambda}}(r))\})\mathrm{d}\Gamma_c \tag{29}$$

with $\bar{\boldsymbol{\Phi}}^\alpha = \bar{\lambda}_t^\alpha \mathbf{I} + \bar{\lambda}_n \mathbf{e}^{\beta\alpha}(\bar{\mathbf{a}}_\beta \times \mathbf{I})$.

It is important to mention that the preceding interface constraint functional will not lead to a standard minimization problem; the reason is that the Coulomb disk $\mathbb{C}_g$ inside the cone projection operator $\mathbb{P}_{\lhd}$ is a function of the normal contact through the friction limit g which depends on the solution $\mathbf{u}$. To overcome this difficulty and following to Alart and Curnier [2] we have obtained a particular form of *quasi*-Lagrangian by substituting g by the convex set $\mu \max(0, \lambda_n)$; for this reason, the minimization problem associated with (16) is considered as a *quasi*-variational problem.

Also note that in Eq. (28) the following terms can be identified:

$$\begin{aligned}
G_{cu}(\boldsymbol{\lambda}; \delta\mathbf{u}) &= \int\int_{\Gamma_c} (\delta\mathbf{u} \cdot \{\mathbf{B}\boldsymbol{\lambda}\})\mathrm{d}\Gamma_c, \\
G_{c\lambda}(\mathbf{x}, \mathbf{y}, \mathbf{k}; \delta\boldsymbol{\lambda}) &= \int\int_{\Gamma_c} (\delta\boldsymbol{\lambda} \cdot \{\mathbf{B}^{\mathbf{t}}(\mathbf{x} - \mathbf{y}) - \mathbf{k}\})\mathrm{d}\Gamma_c, \\
G_{cv}(\mathbf{x}, \mathbf{y}, \boldsymbol{\lambda}; \delta\mathbf{v}) &= \int\int_{\Gamma_c} (-\delta\mathbf{v} \cdot \{\mathbf{B}\boldsymbol{\lambda}\} + \delta\mathbf{v}_{,\alpha} \cdot \{\mathbf{Q}_\alpha \boldsymbol{\Phi}^\alpha(\mathbf{x} - \mathbf{y})\})\mathrm{d}\Gamma_c, \\
G_{ck}(\boldsymbol{\lambda}, \mathbf{k}; \delta\mathbf{k}) &= \int\int_{\Gamma_c} (\delta\mathbf{k} \cdot \{-\boldsymbol{\lambda} + \mathbb{P}_{\lhd}(\boldsymbol{\lambda}(r))\})\mathrm{d}\Gamma_c
\end{aligned} \tag{30}$$

obtaining similar expressions for the barred side (29); where $G_{cu}(\boldsymbol{\lambda}; \delta\mathbf{u})$ represents the virtual work of contact forces acting on the solid Ω, $G_{c\lambda}(\mathbf{x}, \mathbf{y}, \mathbf{k}; \delta\boldsymbol{\lambda})$ constitutes the kinematic constraint between the solid and the frame, $G_{cv}(\mathbf{x}, \mathbf{y}, \boldsymbol{\lambda}; \delta\mathbf{v})$ evaluates the virtual work done by the contact forces on the frame and $G_{ck}(\boldsymbol{\lambda}, \mathbf{k}; \delta\mathbf{k})$ is responsible for the fulfilment of the contact conditions. Once combined these terms with their counterparts from the barred side, the final conditions that will have to be satisfied in the frame are

$$G_{cv}(\mathbf{x}, \mathbf{y}, \boldsymbol{\lambda}; \delta\mathbf{v}) + \overline{G}_{cv}(\bar{\mathbf{x}}, \mathbf{y}, \bar{\boldsymbol{\lambda}}; \delta\mathbf{v}) = 0 \tag{31}$$

or frame equilibrium due to forces coming from both sides and

$$G_{ck}(\boldsymbol{\lambda}, \mathbf{k}; \delta\mathbf{k}) + \overline{G}_{ck}(\bar{\boldsymbol{\lambda}}, \mathbf{k}; \delta\mathbf{k}) = 0 \tag{32}$$

to ensure that those forces, together with the frame displacements, will satisfy the contact conditions.

Special consideration must be taken to the fact that $G_{ck}(\boldsymbol{\lambda}, \mathbf{k}; \delta\mathbf{k})$ and $\overline{G}_{ck}(\bar{\boldsymbol{\lambda}}, \mathbf{k}; \delta\mathbf{k})$ terms are both non-F-differentiable functions.[1] The reason is that there are certain points where a conventional derivative can not be computed; exactly at the change of contact state frontiers. However, in those points the directional derivative can be computed because (32) is a B-differentiable function.

6. Discrete equations

The discrete contact problem will be defined in terms of *contact pairs*, i.e. couples formed by a boundary node and its associated frame element. Those contact pairs are established before starting each time step, calculating for every potentially contacting boundary node its nearest frame element and projecting geometrically on it, see Fig. 5.

The frame displacements $\mathbf{v}(\xi_1, \xi_2)$ and its average distance to the solids $\mathbf{k}(\xi_1, \xi_2)$ are interpolated using isoparametric finite elements in the following form:

$$\mathbf{v}(\xi_1, \xi_2) = \mathbf{N}(\xi_1, \xi_2) \begin{bmatrix} \mathbf{v}_1 \\ \vdots \\ \mathbf{v}_{n_f} \end{bmatrix}, \quad \mathbf{k}(\xi_1, \xi_2) = \mathbf{N}(\xi_1, \xi_2) \begin{bmatrix} \mathbf{k}_1 \\ \vdots \\ \mathbf{k}_{n_f} \end{bmatrix}, \tag{33}$$

where n_f is the number of nodes in the frame element, and

$$\mathbf{N}(\xi_1, \xi_2) = \begin{bmatrix} N_1 & 0 & 0 & \dots & N_{n_f} & 0 & 0 \\ 0 & N_1 & 0 & \dots & 0 & N_{n_f} & 0 \\ 0 & 0 & N_1 & \dots & 0 & 0 & N_{n_f} \end{bmatrix} \tag{34}$$

is the shape functions approximation matrix.

The choice for multiplier discretization is to model them as concentrated forces, that is, support functions are *Dirac's* delta functions

$$\boldsymbol{\lambda}(\xi_1, \xi_2) = \boldsymbol{\lambda}_p \cdot \delta(\boldsymbol{\xi} - \boldsymbol{\xi}_p) \tag{35}$$

with $\boldsymbol{\xi} = (\xi_1, \xi_2)$ and $\boldsymbol{\xi}_p$ the frame coordinates of the node projection, Fig. 5. This definition of contact forces will reduce integrations over the contact zone to summations over the contact pairs, i.e.

$$\int\int_{\Gamma_c} \boldsymbol{\lambda}(\xi_1, \xi_2) \cdot \mathbf{f}(\xi_1, \xi_2)\mathrm{d}\Gamma_c = \sum_{p=1}^{n_p} \boldsymbol{\lambda}_p \cdot \mathbf{f}(\boldsymbol{\xi}_p) \tag{36}$$

with n_p the total number of contact pairs. Expression (36) is useful in order to maintain the contact interface generic, leading to modular coupling software since the frame needs to know very little information about the contacting solids.

To manage the discrete variables we have to introduce the substructural interface nodal indicator L, the well known boolean finite element assembling operator defined in the following way:

$$\begin{aligned}
\mathbf{u}_p &= L_{up}\mathbf{u}, \quad \boldsymbol{\lambda}_p = Fx_{\lambda p}\boldsymbol{\lambda}, \\
\mathbf{v}_p &= L_{vp}\mathbf{v}, \quad \mathbf{k}_p = L_{kp}\mathbf{k},
\end{aligned} \tag{37}$$

where $L_{\square p}$ is used to extract the variable associated with a boundary node p from the global vector of unknowns $\square$ with $\square = u, v, \lambda, k$.

Due to the incremental nature of the frictional contact process, the nodal value of the contact variables at the

[1] The concept of B-differentiability is related with the non-linearity of the directional derivative. Only if a function $\mathbf{F}(\mathbf{z})$ is F-differentiable, its derivative at $\mathbf{z}$ in an arbitrary direction $\mathbf{d}$ is linear and satisfies the equation $\partial\mathbf{F}(\mathbf{z}; \mathbf{d}) = \nabla\mathbf{F}(\mathbf{z})\mathbf{d}$, where $\nabla\mathbf{F}(\mathbf{z})$ is the Jacobian matrix.

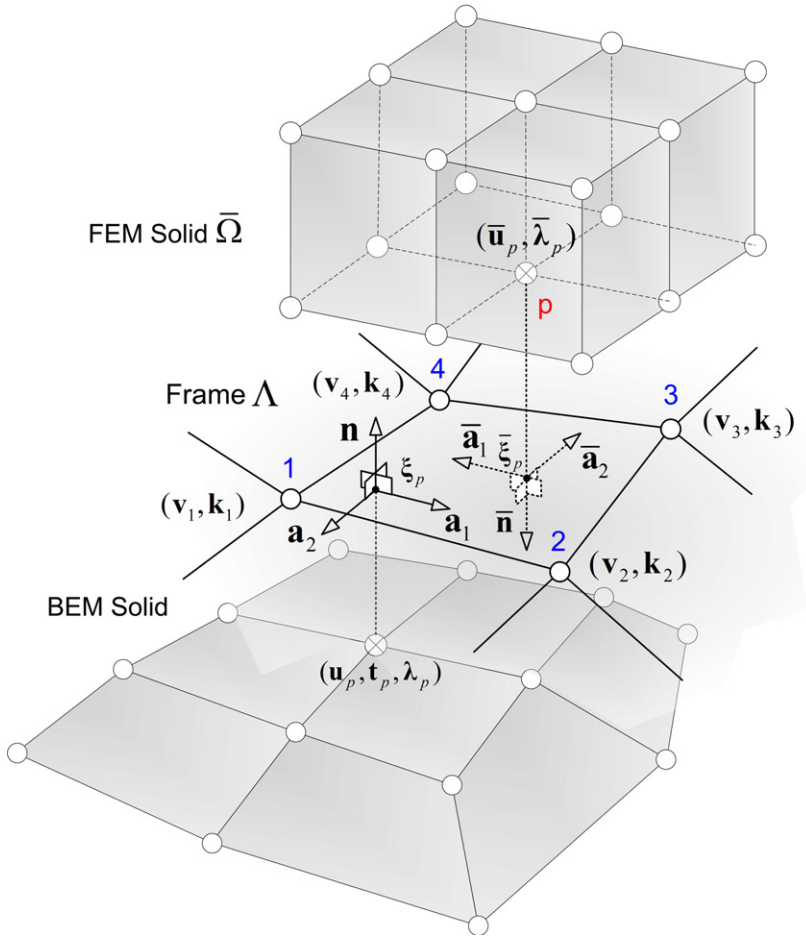

Fig. 5. Each contact pair is constituted by a hitting boundary node p and its closest frame element.

previous time step (t) has to be stored in memory in order to solve for the next time step $(t+\Delta t)$. This is done for the frame displacements $\mathbf{v}^{(t)}$, the average distance of the frame to the solids $\mathbf{k}^{(t)}$, the structural displacements $\mathbf{u}^{(t)}$ and the localized Lagrange multipliers $\boldsymbol{\lambda}^{(t)}$, variables that are arranged in a vector $\mathbf{z}^{(t)} = (\mathbf{u}^{(t)}, \bar{\mathbf{u}}^{(t)}, \boldsymbol{\lambda}^{(t)}, \bar{\boldsymbol{\lambda}}^{(t)}, \mathbf{v}^{(t)}, \mathbf{k}^{(t)})$.

It should be noted that making the variables associated with the contact problem $\mathbf{k}^{(t)}$ and $\mathbf{v}^{(t)}$ to reside in the frame, the contact problem is encapsulated making it easier a substitution of the numerical method used to model the substructures.

6.1. FEM–FEM contact

When the contacting solids are modeled using the FEM, the energy variation of each completely free subsystem can be written in the following general form:

$$\delta\pi^{\text{body}} = \delta\mathbf{u}^{\mathbf{t}} \cdot \{\mathbf{f}^{\text{int}} - \mathbf{f}^{\text{ext}}\}, \tag{38}$$

where $\mathbf{f} = \mathbf{f}^{\text{int}} - \mathbf{f}^{\text{ext}}$ represents the force unbalance or difference between the internal an external forces; expression that when particularized to the linear elastic case is given by $\mathbf{f} = \mathbf{K}\mathbf{u} - \mathbf{f}^{\text{ext}}$.

Using previous definitions, the discrete form of the total FEM–FEM energy functional variation $\delta\Pi^{\text{FF}}$ can be finally written

$$\delta\Pi^{\text{FF}} = \delta\mathbf{u}^{\mathbf{t}} \cdot \mathbf{f} + \delta\bar{\mathbf{u}}^{\mathbf{t}} \cdot \bar{\mathbf{f}} + \delta\boldsymbol{\lambda}^{\mathbf{t}} \cdot \mathbf{g} + \delta\bar{\boldsymbol{\lambda}}^{\mathbf{t}} \cdot \bar{\mathbf{g}} - \delta\mathbf{v}^{\mathbf{t}} \cdot (\mathbf{q} + \bar{\mathbf{q}}) + \delta\mathbf{k}^{\mathbf{t}} \cdot (\mathbf{p} + \bar{\mathbf{p}}), \tag{39}$$

where

$$\mathbf{f} = \sum_{p=1}^{n_p} L^t_{up}\mathbf{f}_p, \quad \mathbf{g} = \sum_{p=1}^{n_p} L^t_{\lambda p}\mathbf{g}_p, \quad \mathbf{q} = \sum_{p=1}^{n_p} L^t_{vp}\mathbf{q}_p, \quad \mathbf{p} = \sum_{p=1}^{n_p} L^t_{kp}\mathbf{p}_p \tag{40}$$

with equivalent definitions for the barred quantities.

For each contact pair, following equations hold

$$\mathbf{f}_p = \{\mathbf{f}^{\text{int}} - \mathbf{f}^{\text{ext}} + \mathbf{B}\boldsymbol{\lambda}\}_p, \quad \bar{\mathbf{f}}_p = \{\bar{\mathbf{f}}^{\text{int}} - \bar{\mathbf{f}}^{\text{ext}} + \overline{\mathbf{B}}\bar{\boldsymbol{\lambda}}\}_p, \tag{41}$$

$$\mathbf{g}_p = \{\mathbf{B}^{\mathbf{t}}(\mathbf{x} - \mathbf{y}) - \mathbf{N}\mathbf{k}\}_p, \quad \bar{\mathbf{g}}_p = \{\overline{\mathbf{B}}^{\mathbf{t}}(\bar{\mathbf{x}} - \mathbf{y}) - \overline{\mathbf{N}}\bar{k}\}_p, \tag{42}$$

$$\mathbf{q}_p = \{-\mathbf{N}^{\mathbf{t}}\mathbf{B}\lambda + \mathbf{N}^{\mathbf{t}}_{,\alpha}\mathbf{Q}_\alpha\boldsymbol{\Phi}^\alpha(\mathbf{x} - \mathbf{y})\}_p,$$

$$\bar{\mathbf{q}}_p = \{-\overline{\mathbf{N}}^{\mathbf{t}}\overline{\mathbf{B}}\bar{\lambda} + \overline{\mathbf{N}}^{\mathbf{t}}_{,\alpha}\overline{\mathbf{Q}}_\alpha\bar{\boldsymbol{\Phi}}^\alpha(\bar{\mathbf{x}} - \mathbf{y})\}_p, \tag{43}$$

$$\mathbf{p}_p = \{\mathbf{N}^{\mathbf{t}}(-\boldsymbol{\lambda} + \mathbb{P}_\triangleleft(\boldsymbol{\lambda}(r)))\}_p, \quad \bar{\mathbf{p}}_p = \{\overline{\mathbf{N}}^{\mathbf{t}}(-\bar{\boldsymbol{\lambda}} + \mathbb{P}_\triangleleft(\bar{\boldsymbol{\lambda}}(r)))\}_p, \tag{44}$$

where Eq. (41) represents the equilibrium equation of each substructure (term $-\mathbf{B}\boldsymbol{\lambda}$ are the contact forces expressed in the global system), Eq. (42) governs the relative motion between the frame and the substructures, Eq. (43) evaluates the forces acting on the frame and Eq. (44) imposes the fulfilment of the contact conditions.

The stationary of the above FEM–FEM variational equation, viz., $\delta\Pi^{\mathrm{FF}} = 0$ is obtained by solving for the group of unknowns $\mathbf{z} = (\mathbf{u}, \bar{\mathbf{u}}, \boldsymbol{\lambda}, \bar{\boldsymbol{\lambda}}, \mathbf{v}, \mathbf{k})$ the following non-linear and B-differentiable system:

$$\mathbf{F}^{\mathrm{FF}}(\mathbf{z}^{(t+\Delta t)}) = \begin{bmatrix} \mathbf{f} \\ \bar{\mathbf{f}} \\ \mathbf{g} \\ \bar{\mathbf{g}} \\ -\mathbf{q} - \bar{\mathbf{q}} \\ \mathbf{p} + \bar{\mathbf{p}} \end{bmatrix}^{(t+\Delta t)} = 0, \tag{45}$$

where non-F-differentiability occurs because equation $\mathbf{p} + \bar{\mathbf{p}}$ can present a non-linear directional derivative.

The partitioned equations of motion for the frame-based FEM–FEM contact problem are obtained from the Jacobian of system (45), that can be expressed as

$$\begin{bmatrix} \mathbf{K} & \mathbf{0} & \mathbf{B} & \mathbf{0} & -\mathbf{L}_v & \mathbf{0} \\ \mathbf{0} & \overline{\mathbf{K}} & \mathbf{0} & \overline{\mathbf{B}} & -\overline{\mathbf{L}}_v & \mathbf{0} \\ \mathbf{B}^{\mathbf{t}} & \mathbf{0} & \mathbf{0} & \mathbf{0} & -\mathbf{L}_b & -\mathbf{N}_k \\ \mathbf{0} & \overline{\mathbf{B}}^{\mathbf{t}} & \mathbf{0} & \mathbf{0} & -\overline{\mathbf{L}}_b & -\overline{\mathbf{N}}_k \\ -\mathbf{L}_v^{\mathbf{t}} & -\overline{\mathbf{L}}_v^{\mathbf{t}} & -\mathbf{L}_b^{\mathbf{t}} & -\overline{\mathbf{L}}_b^{\mathbf{t}} & -\mathbf{D}_v - \overline{\mathbf{D}}_v & \mathbf{0} \\ \mathbf{0} & \mathbf{0} & \mathbf{P}_\lambda & \overline{\mathbf{P}}_\lambda & \mathbf{0} & \mathbf{P}_k + \overline{\mathbf{P}}_k \end{bmatrix} \begin{bmatrix} \Delta\mathbf{u}^{(t)} \\ \Delta\bar{\mathbf{u}}^{(t)} \\ \Delta\boldsymbol{\lambda}^{(t)} \\ \Delta\bar{\boldsymbol{\lambda}}^{(t)} \\ \Delta\mathbf{v}^{(t)} \\ \Delta\mathbf{k}^{(t)} \end{bmatrix} = \begin{bmatrix} -\mathbf{f} \\ -\bar{\mathbf{f}} \\ -\mathbf{g} \\ -\bar{\mathbf{g}} \\ \mathbf{q} + \bar{\mathbf{q}} \\ -\mathbf{p} - \bar{\mathbf{p}} \end{bmatrix}^{(t)}, \tag{46}$$

where only the non-differentiable terms $\mathbf{P}_\lambda$, $\overline{\mathbf{P}}_\lambda$, $\mathbf{P}_k$ and $\overline{\mathbf{P}}_k$ need a special treatment.

Components of the previous system for non-barred quantities are obtained assembling contributions of each contact pair p

$$\begin{aligned} \mathbf{B} &= \sum_{p=1}^{n_p} L_{up}^t \mathbf{B}_p L_{\lambda p}, \quad \mathbf{L}_v = \sum_{p=1}^{n_p} L_{up}^t \mathbf{L}_{vp} L_{vp}, \\ \mathbf{L}_b &= \sum_{p=1}^{n_p} L_{\lambda p}^t \mathbf{L}_{bp} L_{vp}, \quad \mathbf{N}_k = \sum_{p=1}^{n_p} L_{\lambda p}^t \mathbf{N}_{kp} L_{kp}, \\ \mathbf{D}_v &= \sum_{p=1}^{n_p} L_{vp}^t \mathbf{D}_{vp} L_{vp}, \quad \mathbf{P}_\lambda = \sum_{p=1}^{n_p} L_{kp}^t \mathbf{P}_{\lambda p} L_{\lambda p}, \\ \mathbf{P}_k &= \sum_{p=1}^{n_p} L_{kp}^t \mathbf{P}_{kp} L_{kp} \end{aligned} \tag{47}$$

with sums extended to the n_p contact pairs from that side and where each term comes from differentiation of Eqs. (41)–(44)

$$\mathbf{L}_{vp} = \left\{ -(\boldsymbol{\Phi}^\alpha)^{\mathbf{t}} \mathbf{Q}_\alpha \mathbf{N}_{,\alpha} \right\}_p, \tag{48}$$

$$\mathbf{L}_{bp} = \left\{ \mathbf{B}^{\mathbf{t}}\mathbf{N} - \begin{bmatrix} -(\mathbf{x}-\mathbf{y})^t(\mathbf{a}_2 \times \mathbf{I}) \\ (\mathbf{x}-\mathbf{y})^t \\ \mathbf{0} \end{bmatrix} \mathbf{Q}_1 \mathbf{N}_{,1} - \begin{bmatrix} (\mathbf{x}-\mathbf{y})^t(\mathbf{a}_1 \times \mathbf{I}) \\ \mathbf{0} \\ (\mathbf{x}-\mathbf{y})^t \end{bmatrix} \mathbf{Q}_2 \mathbf{N}_{,2} \right\}_p, \tag{49}$$

$$\mathbf{N}_{kp} = \{\mathbf{N}\}_p, \tag{50}$$

$$\begin{aligned} \mathbf{D}_{vp} = \Big\{ & \mathbf{N}^{\mathbf{t}}[(\boldsymbol{\Phi}^\alpha)^{\mathbf{t}} \mathbf{Q}_\alpha] \mathbf{N}_{,\alpha} + \mathbf{N}_{,\alpha}^{\mathbf{t}} [\mathbf{Q}_\alpha \boldsymbol{\Phi}^\alpha] \mathbf{N} \\ & + \mathbf{N}_{,\alpha}^{\mathbf{t}} \frac{1}{\|\mathbf{y}_{,\alpha}\|} \{ \mathbf{Q}_\alpha \boldsymbol{\Phi}^\alpha (\mathbf{x}-\mathbf{y}) \otimes \mathbf{a}_\alpha + \mathbf{a}_\alpha \\ & \otimes \mathbf{Q}_\alpha \boldsymbol{\Phi}^\alpha (\mathbf{x}-\mathbf{y}) + [\boldsymbol{\Phi}^\alpha (\mathbf{x}-\mathbf{y})] \cdot \mathbf{a}_\alpha \mathbf{Q}_\alpha \} \mathbf{N}_{,\alpha} \} \Big\}_p \end{aligned} \tag{51}$$

obtaining similar expressions for the barred side.

On the other hand, terms $\mathbf{P}_{\lambda p}$ and $\overline{\mathbf{P}}_{\lambda p}$ are decomposed into their normal and tangential parts

$$\mathbf{P}_{\lambda p} = \mathbf{P}_{\lambda_n p} + \mathbf{P}_{\lambda_t p} \quad \text{and} \quad \mathbf{P}_{kp} = \mathbf{P}_{k_n p} + \mathbf{P}_{\lambda_t p} \tag{52}$$

with following definition for the normal part:

(1) Case $\lambda_n(r) < 0$

$$\mathbf{P}_{\lambda_n p} = \left\{ \mathbf{N}^{\mathbf{t}} \begin{bmatrix} -1 & 0 & 0 \\ 0 & 0 & 0 \\ 0 & 0 & 0 \end{bmatrix} \right\}_p.$$

(2) Case $\lambda_n(r) \geqslant 0$

$$\mathbf{P}_{k_n p} = \left\{ \mathbf{N}^{\mathbf{t}} \begin{bmatrix} r & 0 & 0 \\ 0 & 0 & 0 \\ 0 & 0 & 0 \end{bmatrix} \mathbf{N} \right\}_p,$$

where we can see that instead of calculating a complicated non-linear directional derivative for the non-differentiable case $\lambda_n(r) = 0$, it has been replaced by a more simple linear derivative coming from the right side. A similar technique is used for non-differentiable points of the tangential contribution:

(1) Case $\lambda_n \leqslant 0$

$$\mathbf{P}_{\lambda_t p} = \left\{ \mathbf{N}^{\mathbf{t}} \begin{bmatrix} 0 & 0 & 0 \\ 0 & -1 & 0 \\ 0 & 0 & -1 \end{bmatrix} \right\}_p.$$

(2) Case $\lambda_n > 0$

(a) When $\|\boldsymbol{\lambda}_t(r)\| \leqslant \mu\lambda_n$

$$\mathbf{P}_{k_t p} = \left\{ \mathbf{N}^{\mathbf{t}} \begin{bmatrix} 0 & 0 & 0 \\ 0 & r & 0 \\ 0 & 0 & r \end{bmatrix} \mathbf{N} \right\}_p,$$

(b) otherwise, if $\|\boldsymbol{\lambda}_t(r)\| > \mu\lambda_n$

$$\mathbf{P}_{\lambda_t p} = \left\{ \mathbf{N}^{\mathbf{t}} \begin{bmatrix} 0 & 0 & 0 \\ \hat{\alpha}\frac{\lambda_t^1(r)}{\lambda_n} & \Psi_{11} & \Psi_{12} \\ \hat{\alpha}\frac{\lambda_t^2(r)}{\lambda_n} & \Psi_{21} & \Psi_{22} \end{bmatrix} \right\}_p,$$

$$\mathbf{P}_{k_t p} = \left\{ \mathbf{N}^{\mathbf{t}} \begin{bmatrix} 0 & 0 & 0 \\ 0 & r\Theta_{11} & r\Theta_{12} \\ 0 & r\Theta_{21} & r\Theta_{22} \end{bmatrix} \mathbf{N} \right\}_p$$

with $\hat{\alpha} = \frac{\mu\lambda_n}{\|\boldsymbol{\lambda}_t(r)\|}$, $\hat{\beta} = \frac{\mu\lambda_n}{[\lambda_t^1(r)^2 + \lambda_t^2(r)^2]^{\frac{3}{2}}}$, $\boldsymbol{\Psi} = (\hat{\alpha} - 1)\mathbf{I} - \hat{\beta}\mathbf{R}$, $\boldsymbol{\Theta} = \hat{\alpha}\mathbf{I} - \hat{\beta}\mathbf{R}$ and $\mathbf{R} = \boldsymbol{\lambda}_t(r) \otimes \boldsymbol{\lambda}_t(r)$.

In the previous expressions we are using a linearized substitute for the non-linear directional derivative appearing when any of these equalities hold $\lambda_n = 0$, $\lambda_n(r) = 0$ or $\|\boldsymbol{\lambda}_t(r)\| = \mu\lambda_n$, although the function can be expected to be normally differentiable in the large majority of practical cases.

6.2. BEM–FEM contact

Modularity of the preceding formulation becomes clear when it is extended to make possible a combination of contacting solids modelled using either the FEM or the BEM. For simplicity and without any loss of generality, we focus on the case where the elastic equations of the first solid in contact are obtained using the BEM and the second solid is modeled using the FEM. In a previous work by the authors [14] it was demonstrated that in coupled elastostatic problems without contact conditions, the variational functional of a BE solid $\delta\pi^{\text{body}}$ to be combined with a variational form like (16) can be expressed by adding two terms: the complementary virtual work associated with the BE elastic equations $\delta\pi^{\text{BEM}}$ and an extra term to transform the boundary tractions into forces $\delta\pi^{\text{lump}}$, i.e. $\delta\pi^{\text{body}} = \delta\pi^{\text{BEM}} + \delta\pi^{\text{lump}}$. The first term, associated with the BEM elastic equations, can be written

$$\delta\pi^{\text{BEM}} = \delta\mathbf{t}^{\mathbf{t}} \cdot \{\mathbf{H}\mathbf{u} - \mathbf{G}\mathbf{t} - \mathbf{b}\}, \tag{53}$$

where vectors $\mathbf{t}$ and $\mathbf{u}$ contain the solid boundary tractions and displacements, respectively, $\mathbf{H}$ and $\mathbf{G}$ are the BEM system matrices obtained when assembling elemental contributions and vector $\mathbf{b}$ is a known function of the boundary conditions, see [14] for more details. Those boundary tractions are in equilibrium with the Lagrange multipliers localized in the contact zone applying an energy equivalence principle that produces the following term:

$$\delta\pi^{\text{lump}} = \delta\mathbf{u}^{\mathbf{t}} \cdot \{\mathbf{M}\mathbf{t} + \mathbf{E}\boldsymbol{\lambda}\} \tag{54}$$

with a lumping matrix used to transform tractions into equivalent forces given by

$$\mathbf{M} = \sum_{e=1}^{n_e} L_{te}^{t} \mathbf{M}_e L_{te}, \tag{55}$$

where n_e is the number of boundary elements situated at the interface, L_{te} is the boolean assembling operator used to extract the variables associated with a boundary element e from the global vector of unknowns and

$$\mathbf{M}_e = \int_{\Gamma_e} \mathbf{N}^{\mathbf{T}} \mathbf{N} \mathrm{d}\Gamma_e \tag{56}$$

is the elemental lumping matrix for an element e with boundary Γ_e. Finally and because not all the boundary nodes belong to the contact zone, a boolean matrix $\mathbf{E}$ is used to associate the LLMs with their corresponding global nodes.

Substituting these two new terms into the variational Eq. (39) a different form of the functional variation is obtained for the BEM–FEM coupling case

$$\begin{aligned} \delta\Pi^{\text{BF}} = {} & \delta\mathbf{t}^{\mathbf{t}} \cdot (\mathbf{H}\mathbf{u} - \mathbf{G}\mathbf{t} - \mathbf{b}) + \delta\mathbf{u}^{\mathbf{t}} \cdot (\mathbf{M}\mathbf{t} + \mathbf{E}\lambda) \\ & + \delta\bar{\mathbf{u}}^{\mathbf{t}} \cdot \bar{\mathbf{f}} + \delta\boldsymbol{\lambda}^{\mathbf{t}} \cdot \mathbf{g} + \delta\bar{\boldsymbol{\lambda}}^{\mathbf{t}} \cdot \bar{\mathbf{g}} - \delta\mathbf{v}^{\mathbf{t}} \cdot (\mathbf{q} + \bar{\mathbf{q}}) \\ & + \delta\mathbf{k}^{\mathbf{t}} \cdot (\mathbf{p} + \bar{\mathbf{p}}), \end{aligned} \tag{57}$$

where it should be noted that this new expression does not represent the variation of a potential energy functional.

The stationary of the BEM–FEM variational equation $\delta\Pi^{BF} = 0$ is obtained when solving for a new group of unknowns $\mathbf{z} = (\mathbf{u}, \bar{\mathbf{u}}, \mathbf{t}, \boldsymbol{\lambda}, \bar{\boldsymbol{\lambda}}, \mathbf{v}, \mathbf{k})$ the following B-differentiable system:

$$\mathbf{F}^{BF}(\mathbf{z}^{(t+\Delta t)}) = \begin{bmatrix} \mathbf{h} \\ \bar{\mathbf{f}} \\ \mathbf{m} \\ \mathbf{g} \\ \bar{\mathbf{g}} \\ -\mathbf{q} - \bar{\mathbf{q}} \\ \mathbf{p} + \bar{\mathbf{p}} \end{bmatrix}^{(t+\Delta t)} = 0 \tag{58}$$

with definitions for the first and third equations given by

$$\mathbf{h} = \{\mathbf{H}\mathbf{u} - \mathbf{G}\mathbf{t} - \mathbf{b}\}, \quad \mathbf{m} = \{\mathbf{M}\mathbf{t} + \mathbf{E}\lambda\}, \tag{59}$$

where $\mathbf{h}$ represents the BE elastic equations and $\mathbf{m}$ the lumping procedure from tractions to forces.

So carrying out the stationary conditions of (58) we find the following equilibrium equation set:

$$\begin{bmatrix} \mathbf{H} & \mathbf{0} & -\mathbf{G} & \mathbf{0} & \mathbf{0} & \mathbf{0} & \mathbf{0} \\ \mathbf{0} & \bar{\mathbf{K}} & \mathbf{0} & \mathbf{0} & \bar{\mathbf{B}} & -\bar{\mathbf{L}}_v & \mathbf{0} \\ \mathbf{0} & \mathbf{0} & \mathbf{M} & \mathbf{E} & \mathbf{0} & -\mathbf{L}_v & \mathbf{0} \\ \mathbf{B}^{\mathbf{t}} & \mathbf{0} & \mathbf{0} & \mathbf{0} & \mathbf{0} & -\mathbf{L}_b & -\mathbf{N}_k \\ \mathbf{0} & \bar{\mathbf{B}}^{\mathbf{t}} & \mathbf{0} & \mathbf{0} & \mathbf{0} & -\bar{\mathbf{L}}_b & -\bar{\mathbf{N}}_k \\ -\mathbf{L}_v^{\mathbf{t}} & -\bar{\mathbf{L}}_v^{\mathbf{t}} & \mathbf{0} & -\mathbf{L}_b^{\mathbf{t}} & -\bar{\mathbf{L}}_b^{\mathbf{t}} & -\mathbf{D}_v - \bar{\mathbf{D}}_v & \mathbf{0} \\ \mathbf{0} & \mathbf{0} & \mathbf{0} & \mathbf{P}_\lambda & \bar{\mathbf{P}}_\lambda & \mathbf{0} & \mathbf{P}_k + \bar{\mathbf{P}}_k \end{bmatrix}$$

$$\times \begin{bmatrix} \Delta\mathbf{u}^{(t)} \\ \Delta\bar{\mathbf{u}}^{(t)} \\ \Delta\mathbf{t}^{(t)} \\ \Delta\boldsymbol{\lambda}^{(t)} \\ \Delta\bar{\boldsymbol{\lambda}}^{(t)} \\ \Delta\mathbf{v}^{(t)} \\ \Delta\mathbf{k}^{(t)} \end{bmatrix} = \begin{bmatrix} -\mathbf{h} \\ -\bar{\mathbf{f}} \\ -\mathbf{m} \\ -\mathbf{g} \\ -\bar{\mathbf{g}} \\ \mathbf{q} + \bar{\mathbf{q}} \\ -\mathbf{p} - \bar{\mathbf{p}} \end{bmatrix}^{(t)} \tag{60}$$

a non-symmetrical and strictly non-differentiable system representing the partitioned equations of motion for the frame-based BEM–FEM contact problem.

Note that the BEM–BEM contact case is straightforward using the same approach.

6.3. Generalization to multi-contacts

One of the advantages of using this partitioned formulation, is that the matrix assembling process of systems (46) and (60) can be easily automatized and extended to the case on n contacting bodies with m frames using a general expression written in the following form when all bodies are modelled using the FEM

$$\begin{bmatrix} \mathbf{K} & \mathbf{B} & -\mathbf{L}_v & \mathbf{0} \\ \mathbf{B}^{\mathbf{t}} & \mathbf{0} & -\mathbf{L}_b & -\mathbf{N}_k \\ -\mathbf{L}_v^{\mathbf{t}} & -\mathbf{L}_b^{\mathbf{t}} & -\mathbf{D}_v & \mathbf{0} \\ \mathbf{0} & \mathbf{P}_\lambda & \mathbf{0} & \mathbf{P}_k \end{bmatrix} \begin{bmatrix} \Delta\mathbf{u}^{(t)} \\ \Delta\boldsymbol{\lambda}^{(t)} \\ \Delta\mathbf{v}^{(t)} \\ \Delta\mathbf{k}^{(t)} \end{bmatrix} = \begin{bmatrix} -\mathbf{f} \\ -\mathbf{g} \\ \mathbf{q} \\ -\mathbf{p} \end{bmatrix}^{(t)}, \tag{61}$$

where $\mathbf{K} = \mathrm{diag}(\mathbf{K}_1, \mathbf{K}_2, \ldots, \mathbf{K}_n)$, $\mathbf{B} = \mathrm{diag}(\mathbf{B}_1, \mathbf{B}_2, \ldots, \mathbf{B}_n)$, $\mathbf{D}_v = \mathrm{diag}(\mathbf{D}_{v1}, \mathbf{D}_{v2}, \ldots, \mathbf{D}_{vm})$ and $\mathbf{P}_k = \mathrm{diag}(\mathbf{P}_{k1}, \mathbf{P}_{k2}, \ldots, \mathbf{P}_{km})$ are diagonal block matrices and $\mathbf{L}_v$, $\mathbf{L}_b$ and $\mathbf{N}_k$ are $n \times m$ block matrices with sub-block (i,j) different from zero if solid i is connected with frame j. A slightly more complicated multi-block matrix is obtained when mixing the FEM and the BEM.

It is also interesting to note that systems (46) and (61) will be only symmetric when all contact points are separated or in a non-contact condition, this makes $\mathbf{P}_\lambda = -\mathbf{N}_k^{\mathbf{t}}$. In contrast to other formulations, mortar-like methods for example, non-symmetry of Eq. (61) comes from the contact conditions but not from the interface treatment.

7. Solving the non-linear system

To solve systems (45) and (58) the Generalized Newton's Method with Line Search (GNMLS) has been used. GNMLS is an effective extension of the Newton's Method for B-differentiable functions proposed by Pang [22] in a general context and particularized by Alart [1] and Christensen [5] for the contact case. This method is based on the computation of the non-linear directional derivative of the objective function; however, it is well known that in contact problems this non-linear directional derivative rarely needs to be computed and can be substituted by a linearized version without affecting the algorithm convergence; this is the approach adopted obtaining (52).

If we define the scalars $\beta \in (0,1)$, $\sigma \in (0,1/2)$, and $\varepsilon > 0$ but small, the application of GNMLS algorithm to solve the non-linear equations $\mathbf{F}(\mathbf{z}) = 0$, can be summarized in the following steps:

(1) Time integration (t), solve for $\mathbf{z}^{(t+\Delta t)}$ known $\mathbf{z}^{(t)}$.
  (a) Inner GNMLS iterations, loop k.
  (b) Use GMRES to solve for $\Delta\mathbf{z}_k^{(t)}$ in the system $\partial\mathbf{F}(\mathbf{z}_k^{(t)}; \Delta\mathbf{z}_k^{(t)}) = -\mathbf{F}(\mathbf{z}_k^{(t)})$ given by (46), (60) or (61).
  (c) Obtain first integer $m = 1,2,\ldots$ that fulfils $\mathbf{H}(\mathbf{z}_k^{(t)} + \beta^m \Delta\mathbf{z}_k^{(t)}) \leqslant (1 - 2\sigma\beta^m)\mathbf{H}(\mathbf{z}_k^{(t)})$ with $\mathbf{H}(\mathbf{z}) = \frac{1}{2}\mathbf{F}^{\mathbf{t}}(\mathbf{z})\mathbf{F}(\mathbf{z})$.
  (d) Actualize solution $\mathbf{z}_{k+1}^{(t)} = \mathbf{z}_k^{(t)} + \tau_k \Delta\mathbf{z}_k^{(t)}$ with $\tau_k = \beta^m$.
  (e) If $\mathbf{H}(\mathbf{z}_{k+1}^{(t)}) \leqslant \epsilon$ continue, else compute new GNMLS iteration $k \leftarrow k + 1$.
(2) Make $\mathbf{z}^{(t+\Delta t)} = \mathbf{z}_{k+1}^{(t)}$ and solve for next time step $(t) \leftarrow (t + \Delta t)$.

The algorithm uses two nested loops, the external one cares for time marching and the internal loop performs the Newton subiterations. On each one of these subiterations a linear system has to be solved to compute the search direction, where we use a sparse matrix storage scheme combined with the GMRES solver. When a new direction $\Delta\mathbf{z}_k^{(t)}$ is obtained, it is scaled by a factor of τ_k obtained from the decreasing error condition given by step (c).

8. Regularization technique

When constitutive characteristics of the contacting solids are very different, the linear system representing equations of motion (61) can become ill-conditioned affecting the overall GNMLS algorithm convergence. To palliate this effect, present in any contact formulation, improving and accelerating the convergence in those extreme cases, a normalization scheme is proposed based on the scaling of displacements and/or Lagrange multipliers.

8.1. Scaling displacements

If we scale the displacements using the following two linear relations:

$$\begin{aligned} \mathbf{u}^* &= \mathbf{S}_u \mathbf{u}, \\ \bar{\mathbf{u}}^* &= \mathbf{S}_{\bar{u}} \bar{\mathbf{u}} \end{aligned} \tag{62}$$

once substituted this regularization in (39), the new expression for the FEM–FEM equations of motion is

$$\begin{bmatrix} \mathbf{S}_u^{\mathbf{t}}\mathbf{K}\mathbf{S}_u & \mathbf{0} & \mathbf{S}_u^{\mathbf{t}}\mathbf{B} & \mathbf{0} & -\mathbf{S}_u^{\mathbf{t}}\mathbf{L}_v & \mathbf{0} \\ \mathbf{0} & \mathbf{S}_{\bar{u}}^{\mathbf{t}}\bar{\mathbf{K}}\mathbf{S}_{\bar{u}} & \mathbf{0} & \mathbf{S}_{\bar{u}}^{\mathbf{t}}\bar{\mathbf{B}} & -\mathbf{S}_{\bar{u}}^{\mathbf{t}}\bar{\mathbf{L}}_v & \mathbf{0} \\ \mathbf{B}^{\mathbf{t}}\mathbf{S}_u & \mathbf{0} & \mathbf{0} & \mathbf{0} & -\mathbf{L}_b & -\mathbf{N} \\ \mathbf{0} & \bar{\mathbf{B}}^{\mathbf{t}}\mathbf{S}_{\bar{u}} & \mathbf{0} & \mathbf{0} & -\bar{\mathbf{L}}_b & -\mathbf{N} \\ -\mathbf{L}_v^{\mathbf{t}}\mathbf{S}_u & -\bar{\mathbf{L}}_v^{\mathbf{t}}\mathbf{S}_{\bar{u}} & -\mathbf{L}_b^{\mathbf{t}} & -\bar{\mathbf{L}}_b^{\mathbf{t}} & -\mathbf{D}_v - \bar{\mathbf{D}}_v & \mathbf{0} \\ \mathbf{0} & \mathbf{0} & \mathbf{P}_\lambda & \bar{\mathbf{P}}_\lambda & \mathbf{0} & \mathbf{P}_k + \bar{\mathbf{P}}_k \end{bmatrix} \times \begin{bmatrix} \Delta\mathbf{u}^*(t) \\ \Delta\bar{\mathbf{u}}^*(t) \\ \Delta\boldsymbol{\lambda}^{(t)} \\ \Delta\bar{\boldsymbol{\lambda}}^{(t)} \\ \Delta\mathbf{v}^{(t)} \\ \Delta\mathbf{k}^{(t)} \end{bmatrix} = \begin{bmatrix} -\mathbf{S}_u^{\mathbf{t}}\mathbf{f} \\ -\mathbf{S}_{\bar{u}}^{\mathbf{t}}\bar{\mathbf{f}} \\ -\mathbf{g} \\ -\bar{\mathbf{g}} \\ \mathbf{q} + \bar{\mathbf{q}} \\ -\mathbf{p} - \bar{\mathbf{p}} \end{bmatrix}^{(t)}, \tag{63}$$

where it is clear that among many possible matrix choices for $\mathbf{S}_u$ and $\mathbf{S}_{\bar{u}}$, a diagonal matrix that modifies the first two diagonal entries of (63) making them of the same order would be a simple normalization option. Our choice is then to make $\mathbf{S}_u = \mathrm{diag}(\mathbf{K})^{-\frac{1}{2}}$ for each substructure and to solve for the scaled displacements $\mathbf{u}^*$ instead of the real ones $\mathbf{u}$.

8.2. Scaling displacements and multipliers

Considering that the localized method of Lagrange multipliers utilizes independent Lagrange multipliers for each substructure, that fact will allow us to introduce two independent normalization factors for each group of Lagrange multipliers

$$\begin{aligned} \boldsymbol{\lambda}^* &= \mathbf{S}_\lambda \boldsymbol{\lambda}, \\ \bar{\boldsymbol{\lambda}}^* &= \mathbf{S}_{\bar{\lambda}} \bar{\boldsymbol{\lambda}}, \end{aligned} \tag{64}$$

where $\mathbf{S}_\lambda$ and $\mathbf{S}_{\bar{\lambda}}$ are linear transformations to define. Observe that by taking appropriate values of these matrices we can independently scale the unknown Lagrange multipliers $\boldsymbol{\lambda}$ and $\bar{\boldsymbol{\lambda}}$, and that no such scaling possibility exists when using the classical Lagrange multipliers method.

Substitution of (62) and (64) in (39) gives

$$\begin{bmatrix} \mathbf{S}_u^{\mathrm{t}}\mathbf{K}\mathbf{S}_u & \mathbf{0} & \mathbf{S}_u^{\mathrm{t}}\mathbf{B}\mathbf{S}_\lambda & \mathbf{0} & -\mathbf{S}_u^{\mathrm{t}}\mathbf{L}_v & \mathbf{0} \\ \mathbf{0} & \mathbf{S}_{\bar{u}}^{\mathrm{t}}\bar{\mathbf{K}}S_{\bar{u}} & \mathbf{0} & \mathbf{S}_{\bar{u}}^{\mathrm{t}}\overline{\mathbf{B}S}_{\bar{\lambda}} & -\mathbf{S}_{\bar{u}}^{\mathrm{t}}\overline{\mathbf{L}}_v & \mathbf{0} \\ \mathbf{S}_\lambda^{\mathrm{t}}\mathbf{B}^{\mathrm{t}}\mathbf{S}_u & \mathbf{0} & \mathbf{0} & \mathbf{0} & -\mathbf{S}_\lambda^{\mathrm{t}}\mathbf{L}_b & -\mathbf{S}_\lambda^{\mathrm{t}}\mathbf{N} \\ \mathbf{0} & \mathbf{S}_{\bar{\lambda}}^{\mathrm{t}}\overline{\mathbf{B}}^{\mathrm{t}}\mathbf{S}_{\bar{u}} & \mathbf{0} & \mathbf{0} & -\mathbf{S}_{\bar{\lambda}}^{\mathrm{t}}\overline{\mathbf{L}}_b & -\mathbf{S}_{\bar{\lambda}}^{\mathrm{t}}\mathbf{N} \\ -\mathbf{L}_v^{\mathrm{t}}\mathbf{S}_u & -\overline{\mathbf{L}}_v^{\mathrm{t}}\mathbf{S}_{\bar{u}} & -\mathbf{L}_b^{\mathrm{t}}\mathbf{S}_\lambda & -\overline{\mathbf{L}}_b^{\mathrm{t}}\mathbf{S}_{\bar{\lambda}} & -\mathbf{D}_v - \overline{\mathbf{D}}_v & \mathbf{0} \\ \mathbf{0} & \mathbf{0} & \mathbf{P}_\lambda\mathbf{S}_\lambda & \overline{\mathbf{P}}_\lambda\mathbf{S}_{\bar{\lambda}} & \mathbf{0} & \mathbf{P}_k + \overline{\mathbf{P}}_k \end{bmatrix} \times \begin{bmatrix} \Delta\mathbf{u}^*(t) \\ \Delta\bar{\mathbf{u}}^*(t) \\ \Delta\boldsymbol{\lambda}^*(t) \\ \Delta\bar{\boldsymbol{\lambda}}^*(t) \\ \Delta\mathbf{v}^{(t)} \\ \Delta\mathbf{k}^{(t)} \end{bmatrix} = \begin{bmatrix} -\mathbf{S}_u^{\mathrm{t}}\mathbf{f} \\ -\mathbf{S}_{\bar{u}}^{\mathrm{t}}\bar{\mathbf{f}} \\ -\mathbf{S}_\lambda^{\mathrm{t}}\mathbf{g} \\ -\mathbf{S}_{\bar{\lambda}}^{\mathrm{t}}\bar{\mathbf{g}} \\ \mathbf{q} + \bar{\mathbf{q}} \\ -\mathbf{p} - \bar{\mathbf{p}} \end{bmatrix}^{(t)} \tag{65}$$

and to make terms $\mathbf{S}_u^{\mathrm{t}}\mathbf{B}\mathbf{S}_\lambda \approx 1$ our choice is to define $\mathbf{S}_\lambda = \mathrm{diag}(\mathbf{K})^{\frac{1}{2}}$ for each group of Lagrange multipliers. The effect of this regularization technique is also studied by Park, Felippa and Gumaste in [26,15] for heterogeneous structural systems, where an important acceleration of the iterative solution algorithm was observed.

9. Applications

In this section, four numerical examples are solved to demonstrate the possibilities of the proposed methodology. The first test is classical benchmark in contact problems, the 3D Hertz's contact problem. The second application is a three solids example using the FEM–FEM coupling approach where the material dissimilarity influence on the iterative solution convergence is discussed. The third one is an industrial application; a simplified tire-road contact problem treated using the proposed BEM–FEM coupling technique. The final example is a BEM–BEM contact case where the indentation of a block into a half-space is considered.

9.1. FEM–FEM contact: The Hertz's problem

The problem considered is the Hertzian contact of two geometrically identical elastic spheres of radius $R_1 = R_2 = 8$ indented applying an external load $P = 1$ normal to the contact zone. The material properties for the first sphere are $E_1 = 100$, $\nu_1 = 0.2$ and $E_2 = 100$, $\nu_2 = 0.4$ for the second. This difference in the Poisson's ratio, together with a friction coefficient $\mu = 0.25$ will produce a distribution of tangential stresses in the contact zone that will not affect considerably the normal pressure, which will be very close to the Hertz solution that predicts a contact zone size $a_{\mathrm{Hertz}} = 0.756$ and a maximum contact pressure $p_{\mathrm{Hertz}} = 3.342$.

The mesh of the lower sphere is generated using 1280 hexahedral elements and 1569 nodes, refining the potential contact zone (a square with side length 1) with 100 hexahedrical elements and 121 contact nodes, see Fig. 6. The second sphere is discretized using a similar but coarse mesh of 896 hexahedral elements with only 64 located in the potential contact area. The contact frame is a plane of 1 mm^2 that uses the same discretization as the potential contact zone of the upper sphere.

The normal pressure distribution obtained is presented in Fig. 6 (right-up) where the Hertz solution is well recognized. It is known that the coupling between the normal and tangential stresses for this problem is very low, meaning that normal tractions are not considerably affected by the frictional phenomena. It was also observed that the number of steps used to apply the normal load did not modify the normal solution but affected the tangential tractions inside the central stick zone. Four steps were used to apply the normal load in this case.

Finally, the contact zone tangential stresses in the y direction can be observed in Fig. 6 (right-down) obtaining the same solution but rotated 90° for the orthogonal direction x. It represents a complex slip–stick–slip shape that has to satisfy the slip condition in an external annular region combined with the adhesion state inside.

9.2. FEM–FEM contact: Layer between two blocks

For this test we consider a very soft elastic layer trapped between two elastic blocks and compressed by the effect of a normal constant pressure applied on the top of one of them, see Fig. 7. These two blocks share the same elastic constants E_b and $\nu_b = 0.3$, and the constitutive parameters for the layer are $E_l = 1$ and $\nu_l = 0.3$ together with a friction coefficient $\mu = 0.25$ between both materials. Our interest is to investigate the effect of the stiffness ratio E_b/E_l on the contact forces and the solution algorithm efficiency.

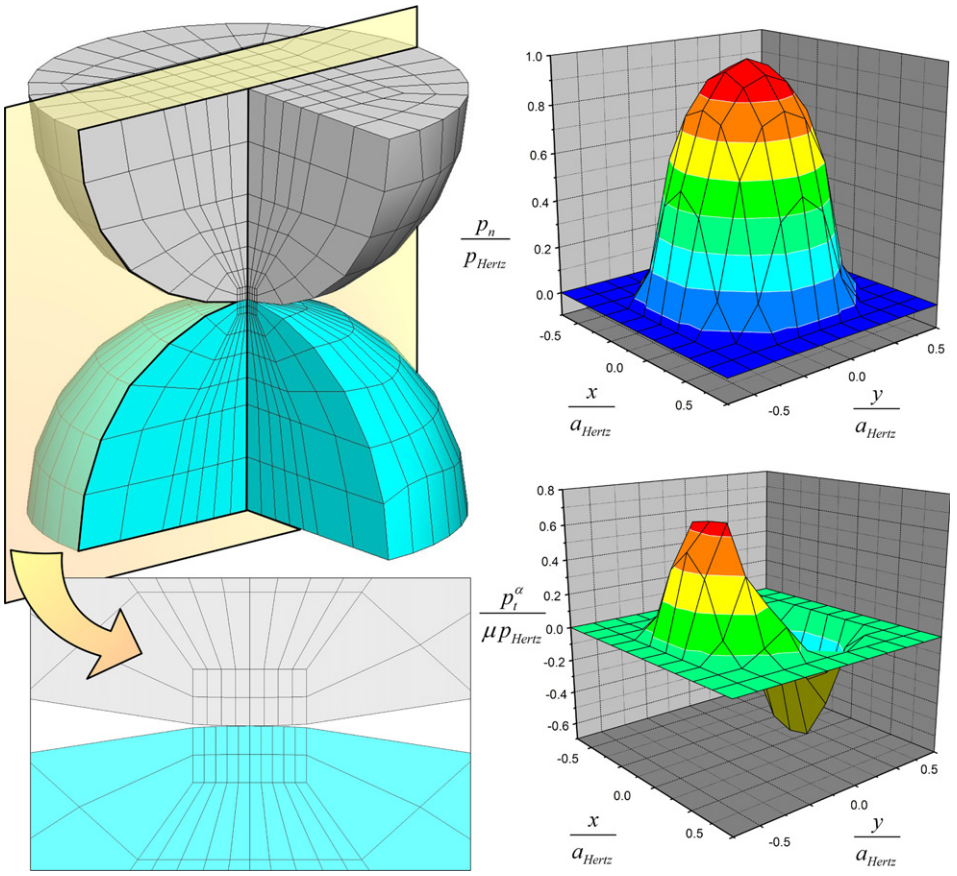

Fig. 6. Three-quarters and section of the mesh used for the Hertzian problem (left), distribution of normal pressure and tangential stresses at the contact zone (right).

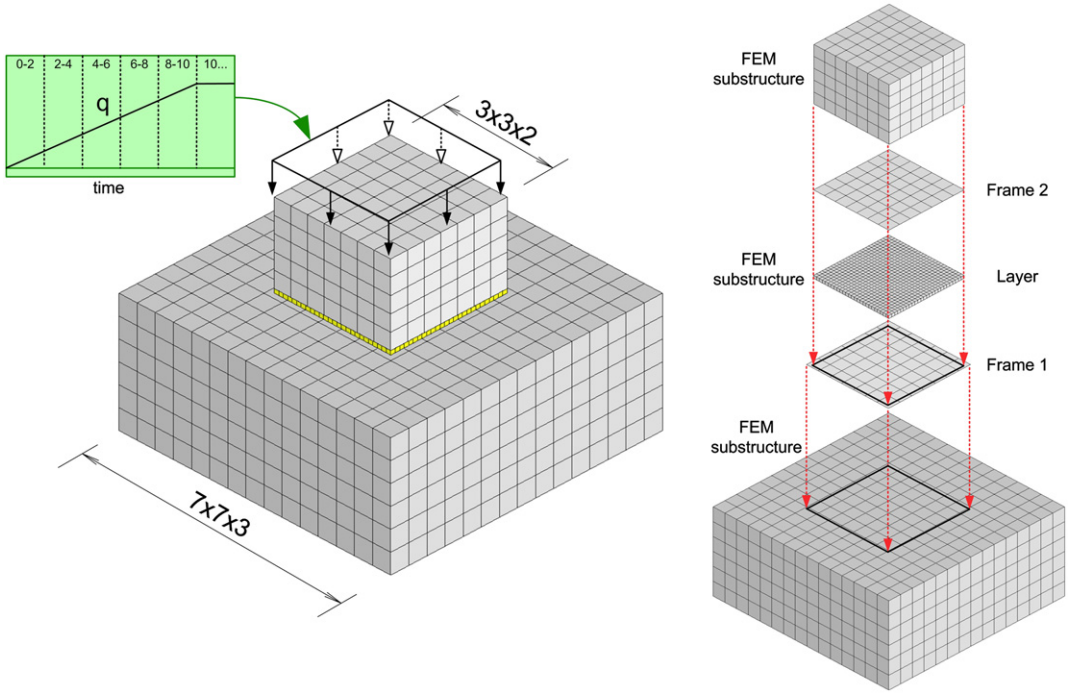

Fig. 7. Mesh of the layer problem and its exploded view with three substructures and two contact frames.

The system is modeled by three substructures and two contact frames between their interfaces. The base block, with dimensions $7 \times 7 \times 3$, is discretized using a regular hexahedrical mesh with 1350 brick elements and connected to the first frame, a plane with 49 quadrilateral linear elements. The layer has a constant thickness $e = 0.1$ and presents a more refined mesh with 1458 brick elements, connected to a second frame with the same discretization than the first one. Finally, the upper block has dimensions $3 \times 3 \times 2$ with a regular hexahedrical mesh of 245 elements and a constant pressure q on the top. This uniform pressure is linearly increased with time and applies a net normal load $P = 0.49$ after ten time steps.

9.2.1. Case $E_b/E_l = 10$

When the relative stiffness between the solids remains small, a distribution of Lagrange multipliers is obtained under the layer that reduces adhesion to the center of the contact area where the normal pressure is lower, Fig. 8. It is well known that normal stresses for the block indentation problem are singular in the border of the contact zone, this effect, however, is not well represented in Fig. 8 because Lagrange multipliers are nodal forces and contributive areas are different for borders and corners than for interior nodes.

For this case, convergence history of the GNMLS algorithm is unproblematic and quite uniform, reaching for the first load step a relative error of 10^{-7} with ten iterations and up to 10^{-13} with forty iterations without using any regularization technique.

9.2.2. Case $E_b/E_l = 1000$

The distribution of contact forces for this case is quite different from the previous one, see Fig. 9, the normal and tangential multipliers become uniform except for a narrow strip around the border of the contact area where the tangential stresses are concentrated. Material dissimilarity causes this strong discontinuity, affecting the

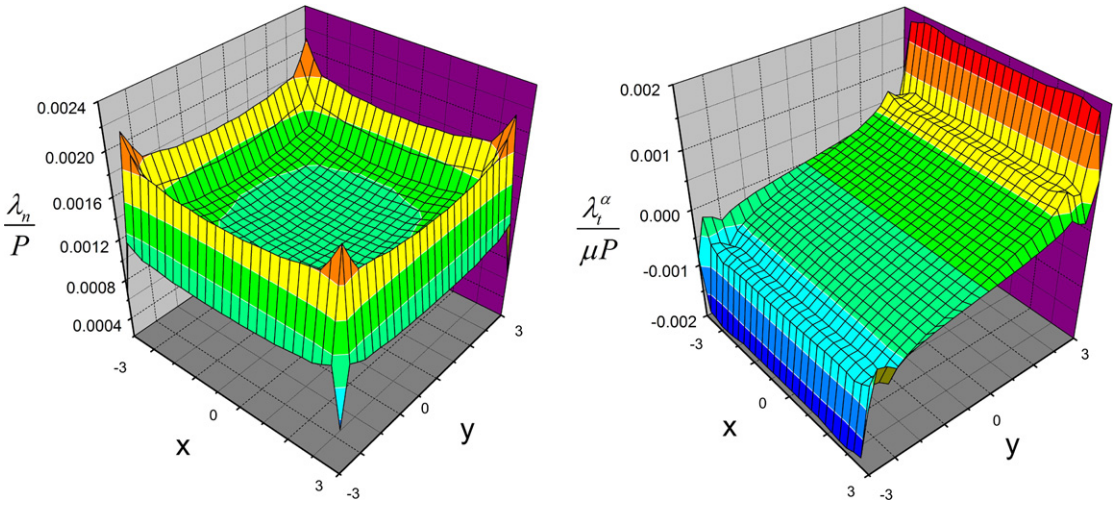

Fig. 8. Normal multipliers (left) and tangential multipliers (right) under the layer for the case $E_b/E_l = 10$.

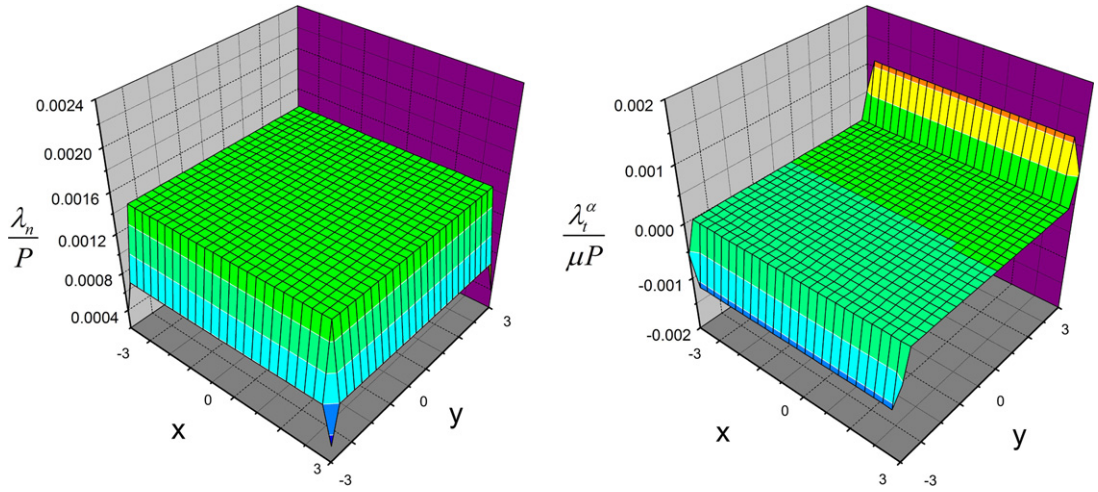

Fig. 9. Normal multipliers (left) and tangential multipliers (right) under the layer for the case $E_b/E_l = 1000$.

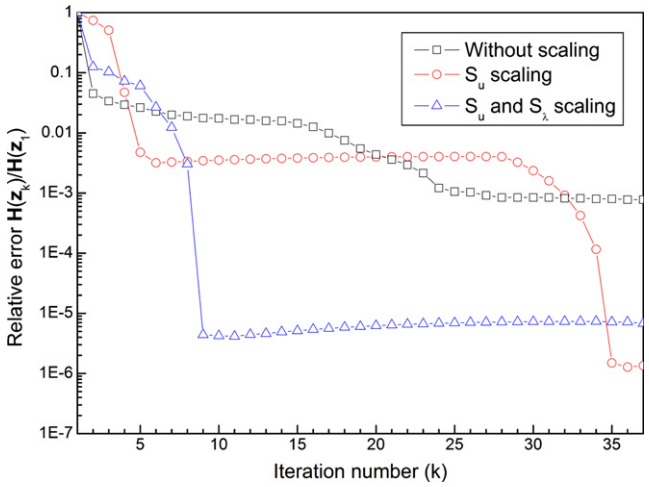

Fig. 10. Effect of the regularization technique on the solution algorithm convergence when $E_b/E_l = 1000$.

GNMLS algorithm convergence. From a mathematical point of view, convergence problems appear due to an ill-condition of the system representing equations of motion and can be reduced using any of the regularization techniques proposed in Section 8.

Observe from Fig. 10 that without using regularizations, almost forty iterations of the GNMLS algorithm are not enough to decrease the relative residual below 10^{-3}. However, if the displacement scaling given by Eq. (63) is used, the algorithm converges to 10^{-6} but needs an important number of iterations. Note that the better convergence results are obtained when combining the displacement and multiplier regularization proposed in Eq. (65), where the same grade of convergence than using the displacement scaling is obtained but much more quickly.

The same behavior was observed by Park et al. [26] for structural systems with both material and geometric heterogeneities, concluding that multipliers regularization accelerates substantially the convergence of iterative solution schemes for partitioned structural systems connected using LLMs.

9.3. BEM–FEM contact: Tire-road contact modelling

Modeling contact phenomena in the tire footprint is a formidable task, partly because of the difficulty of modeling the tire behavior and partly due to the non-linear contact process. Moreover, the complex mechanisms of rolling contact [17,11,12] and dynamic friction which allow the tire to develop the necessary steering and braking forces makes this problem to occupy a position of special interest in engineering mechanics. But our intention here is only to

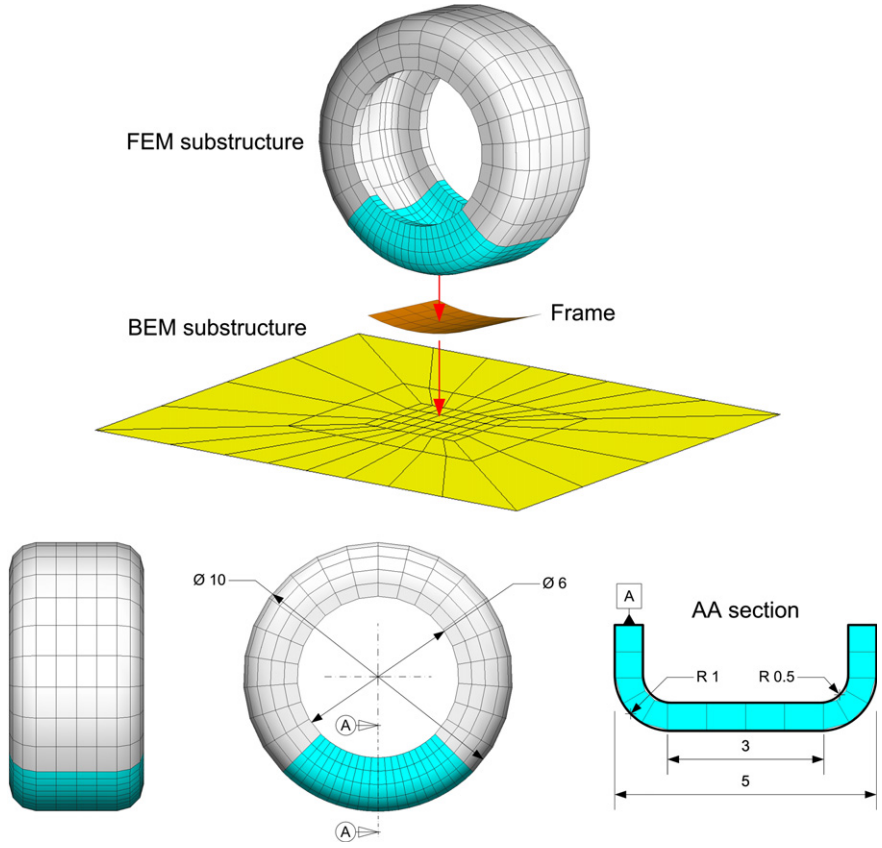

Fig. 11. Perspective with an exploded view of the tire modeled using the FEM, the frame and the BE half-space representing the road (up) and dimensions of the tire (down).

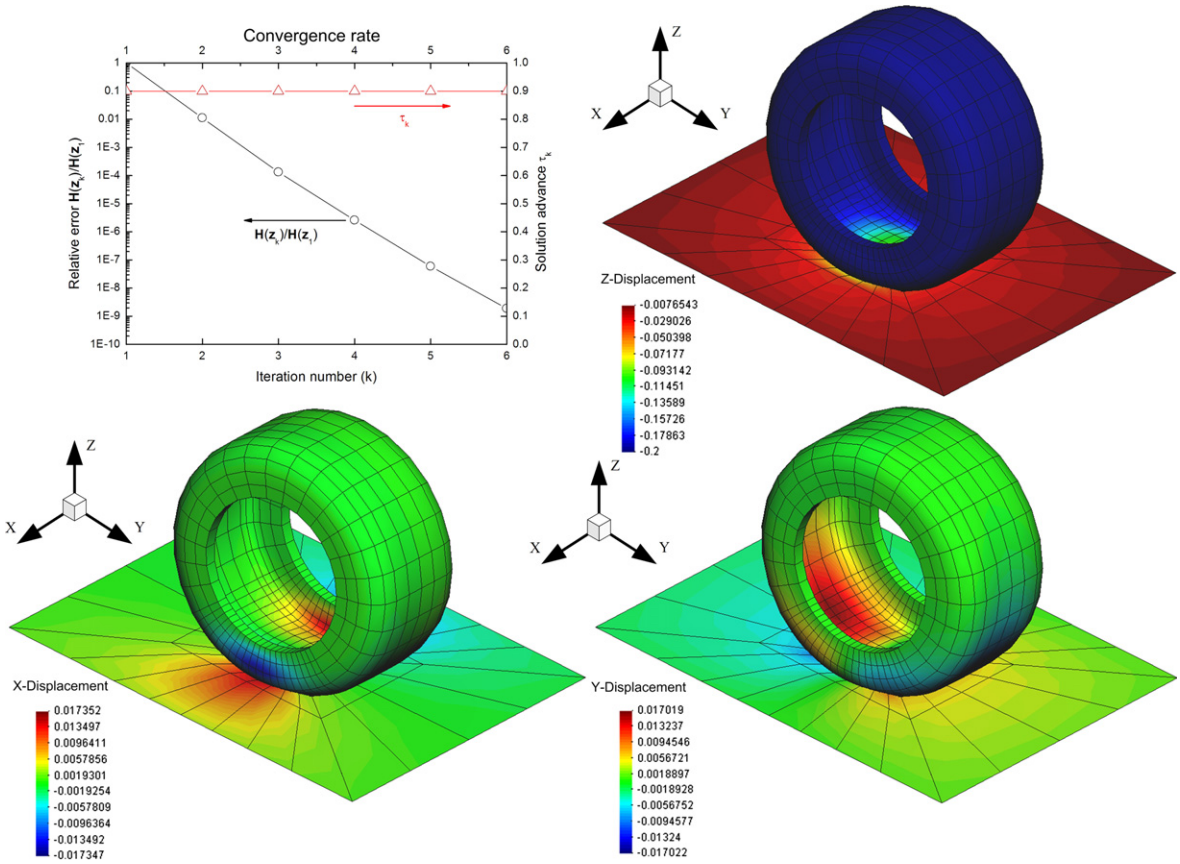

Fig. 12. Displacement fields on the road and the tire when a vertical rigid body displacement is imposed on the wheel.

demonstrate the possibilities of the proposed methodology when applied to this kind of problems by using a simplified example.

In this example we study the case of a stopped tire connected to an infinitely rigid wheel that presents a controlled vertical displacement, imposed on its center axis, making the tire to interact with the ground surface. This problem is usually solved considering the road as an infinitely rigid surface, a good approximation when the stiffness ratio between the tire and the road is small and that liberates the analyst from the necessity of modeling a complete half-space domain with its associated computational cost.

The analysis of the solids is taken under the hypotheses of small deformations and linear elastic behavior of the materials, with constitutive parameters for the tire $E_t = 10$, $v_t = 0.3$ and for the soil $E_s = 1$, $v_s = 0.3$. A comparable stiffness of the materials makes unacceptable substituting the soil by a rigid plane and this is the reason why the BE method is used to approximate the half-space while the tire is modelled using the FEM. In the contact region a static friction coefficient of $\mu = 0.25$ is supposed to simulate the frictional contact conditions.

The dimensions and discretizations used for the solids and the contact frame are presented in Fig. 11; the tire with an external diameter of 10 is discretized using a mesh of 560 hexahedrical finite elements with only one element along the thickness and 1200 nodes with a refined clustering in the vicinity of the contact zone, the frame is modeled using a regular mesh of 32 quadrilateral elements and the elastic half-space with dimensions 14×16 is approximated using a truncated mesh of 80 quadrilateral boundary elements. To capture the stress gradients near the contact zone, a higher density of elements was chosen for specific regions of interest: in the half-space center, the potential contact zone has dimensions 3×3.4 and is discretized using a regular mesh with 32 elements that is almost coincident with the frame mesh, and the tire presents a more refined mesh in the estimated contact zone situated in the region where $-45° \leqslant \theta \leqslant 45°$ with a concentration of 280 bricks.

Fig. 12 shows the displacement contours obtained in the boundary of the solids when a vertical displacement of 0.2 is imposed on the wheel. It is also represented the relative error of the solution obtained by the GNMLS algorithm with the iteration number, presenting a quadratical convergence rate to the solution and reaching a relative error $\mathbf{H}(\mathbf{z}_k)/\mathbf{H}(\mathbf{z}_1)$ of 10^{-9} after only six iterations of the GNLMS algorithm.

9.4. BEM–BEM contact: Indentation with lateral displacement

Indentation with lateral displacement of a block into a half-space is the final elementary test used to highlight

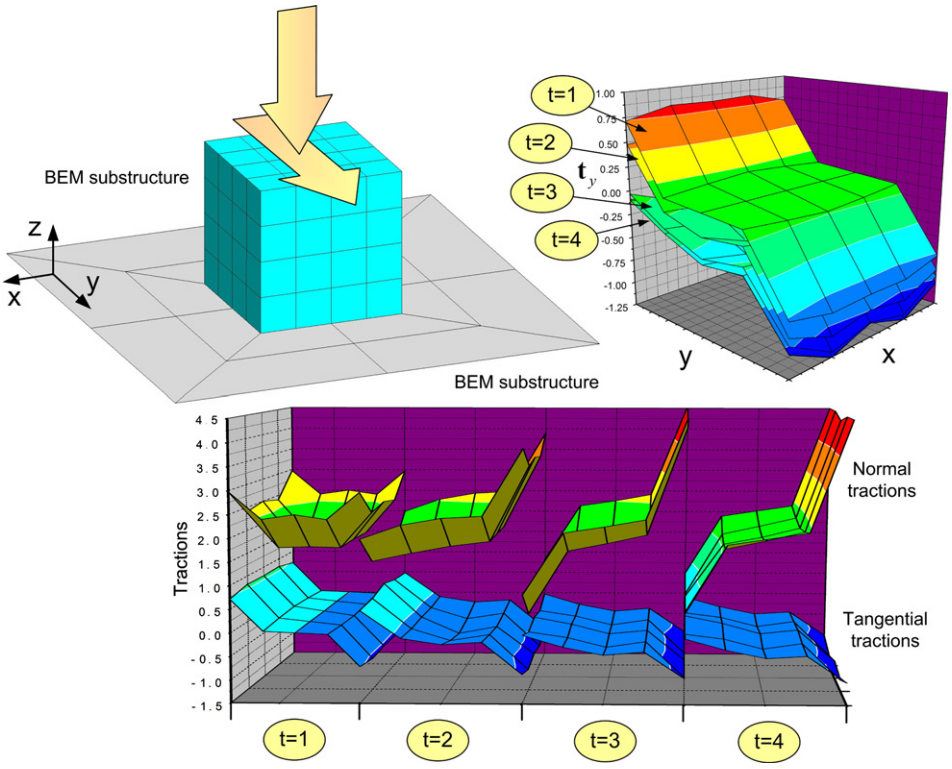

Fig. 13. Mesh used for the indentation problem and interface tractions obtained for different time steps.

the application of the proposed formulation to BEM–BEM contact problems. The block is a cube with side length 0.5 that is discretized using a regular mesh of 96 quadrilateral boundary elements and 98 nodes, see Fig. 13. The frame is composed by four quadrilateral elements and the elastic half-space, discretized using a square truncated mesh with side length 1.5, is approximated using 20 quadrilateral boundary elements and 25 nodes. The material coefficients chosen for this simulation are $E_1 = 100$, $\nu_1 = 0.3$ for the block and $E_2 = 1000$, $\nu_2 = 0.4$ for the half-space, together with a friction coefficient $\mu = 0.25$ between them.

Displacement boundary conditions are imposed on the top face of the block. First, a constant vertical displacement $u_z = -0.01$ produces the indentation and later an increasing lateral displacement on the y direction $u_y = 0.005(1 - t)$ is applied for $t \geqslant 1$.

Normal and tangential tractions under the block for different time steps are also represented in Fig. 13. In the solution for $t = 1$, when no lateral displacement exists, the outside corners of the block experience nearly singular stresses that are damped by the coarse mesh used. When the lateral displacement begins $t = 2,3,4$ the block starts to slip across the half-space with the normal tractions increasing under the leading edge of the contact zone and decreasing through the trailing edge. It is at time $t = 4$ that all the contact zone is under the slip condition, with negative values of the tangential tractions opposed to the direction of motion.

10. Conclusions

A unified formulation combining the BEM and FEM in 3D frictional contact problems using LLMs to connect the different substructures to an adaptative contact frame is presented. The contact conditions are imposed mathematically using projection functions and the contact frame is allowed to move freely between the substructures maintaining the contact zone as an unknown. The GNMLS is applied to solve the non-smooth system of equations representing the equations of motion and different regularization techniques to improve convergence are proposed and tested.

Small displacements are considered when introducing the equations of motion of the FEM or BEM solids but this assumption is relaxed to obtain the equations of motion of the contact frame. Large displacements or an extension of the formulation to large slip contact problems would require an algorithm to update the contact frame geometry [27] and to redefine the group of contacting pairs every time that new nodes of the solids come inside or leave the contact frame. However, these added complexities do not affect the contact treatment that will remain completely valid.

Although other alternatives exist, like the mortar method where continuity conditions are transmitted through an optimal approximation space, the support functions used to approximate the LLMs combined with a contact frame endowed with the contact variables affects

considerably the modularity of the final formulation. This combination allows to isolate the contact problem from the substructures becoming independent of the numerical method used to model them. In our opinion, any nodal based numerical scheme used to simulate the behavior of the substructures could be easily connected with the contact frame as well.

The algorithm and introduced formulations prove to be very robust and efficient when solving 3D non-matching contact problems with small displacements, even when presenting strong material heterogeneities and BEM–FEM transitions trough the contact zone. Suggested methodology greatly simplifies the procedure to solve this kind of problems, minimizing the geometrical knowledge of the contacting substructures needed to formulate the contact interface behavior.

Acknowledgement

The present work has been supported by the *Ministerio de Ciencia y Tecnología* of Spain under the contract number DPI2003-00487.

References

[1] P. Alart, Méthode de newton généralisée en mécanique du contact, J. Math. Pures Appl. (76) (1997) 83–108.
[2] P. Alart, A. Curnier, A mixed formulation for frictional contact problems prone to newton like solution methods, Comp. Appl. Mech. Engrg. 32 (1991) 353–475.
[3] F.B. Belgacem, P. Hild, P. Laborde, The mortar finite element method for contact problems, Mathl. Comput. Model. 28 (4–8) (1998) 263–271.
[4] C.A. Brebbia, P. Georgiou, Combination of boundary and finite elements for elastostatics, Appl. Math. Model. (3) (1979) 212–220.
[5] P.W. Christensen, A. Klarbring, J.S. Pang, N. Strömberg, Formulation and comparison of algorithms for frictional contact problems, Int. J. Numer. Methods Engrg. 42 (1998) 145–173.
[6] M.A. Crisfield, Re-visiting the contact patch test, Int. J. Numer. Methods Engrg. (48) (2000) 435–449.
[7] G. DeSaxe, Z.W. Feng, New inequality and functional for contact with friction: the implicit standard approach, Mech. Struct. Mach. 19 (1991) 301–325.
[8] Y. Ezawa, N. Okamoto, Development of contact stress analysis programs using the hybrid method of FEM and BEM, Comput. Struct. 58 (1) (1996) 13–20.
[9] K.A. Fisher, P. Wriggers, Frictionless 2d contact formulations for finite deformations based on the mortar method, Comput. Mech. (36) (2005) 226–244.
[10] B. Flemisch, M.A. Puso, B.I. Wohlmuth, A new dual mortar method for curved interfaces: 2d elasticity, Int. J. Numer. Methods Engrg. (63) (2005) 813–832.
[11] J.A. González, R. Abascal, An algorithm to solve coupled 2d rolling contact problems, Int. J. Numer. Methods Engrg 49 (2000) 1143–1167.
[12] J.A. González, R. Abascal, Solving 2d transient rolling contact problems using the bem and mathematical programming, Int. J. Numer. Methods Engrg 53 (2002) 843–874.
[13] J.A. González, K.C. Park, C.A. Felippa, Partitioned formulation of frictional contact problems using localized Lagrange multipliers, Commun. Numer. Methods Engrg. (22) (2005) 319–333.
[14] J.A. González, K.C. Park, C.A. Felippa, FEM and BEM coupling in elastostatics using localized Lagrange multipliers, Int. J. Numer. Methods Engrg. (2006).
[15] U.A. Gumaste, K.C. Park, C.A. Felippa, A family of partitioned time integration algorithms for parallel analysis of heterogeneous structural systems, Comput. Mech. (24) (2000) 463–475.
[16] P. Hild, Numerical implementation of two nonconforming finite element method for unilateral contact, Comput. Methods Appl. Mech. Engrg. (184) (2000) 99–123.
[17] G.D. Hu, P. Wriggers, On the adaptive finite element method of steady-state rolling contact for hyperelasticity in finite deformations, Comput. Methods Appl. Mech. Engrg. (191) (2002) 1333–1348.
[18] T.J.R. Hughes, R.L. Taylor, J.L. Sackman, A. Curnier, W. Kanoknukulchai, A finite element method for a class of contact-impact problems, Comput. Methods Appl. Mech. Engrg. (8) (1976) 249–276.
[19] T.A. Laursen, Computational Contact and Impact Mechanics, Fundamentals of Modeling Interfacial Phenomena in Nonlinear Finite Element Analysis, Springer, Berlin, Heidelberg, New York, 2002.
[20] T.W. McDevitt, T.A. Laursen, A mortar finite element formulation for frictional contact problems, Int. J. Numer. Methods Engrg. (48) (2000) 1525–1547.
[21] C. Oysu, R.T. Fenner, Coupled FEM–BEM for elastoplastic contact problems using Lagrange multipliers, Appl. Math. Model. 30 (3) (2006) 231–247.
[22] J.S. Pang, Newton's method for B-differentiable equations, Math. Oper. Res. 15 (2) (1990) 311–341.
[23] P. Papadopoulos, R.L. Taylor, A mixed formulation for the finite element solution of contact problems, Comput. Methods Appl. Mech. Engrg. (94) (1992) 373–384.
[24] K.C. Park, C.A. Felippa, A variational framework for solution method developments in structural mechanics, J. Appl. Mech. (65) (1998) 242–249.
[25] K.C. Park, C.A. Felippa, A variational principle for the formulation of partitioned structural systems, Int. J. Numer. Methods Engrg. (47) (2000) 395–418.
[26] K.C. Park, C.A. Felippa, U.A. Gumaste, A localized version of the method of Lagrange multipliers and its applications, Comput. Mech. (24) (2000) 476–490.
[27] K.C. Park, C.A. Felippa, G. Rebel, A simple algorithm for localized construction of non-matching structural interfaces, Int. J. Numer. Methods Engrg. (53) (2002) 2117–2142.
[28] M.A. Puso, T.A. Laursen, A mortar segment-to-segment contact method for large deformation solid mechanics, Comput. Methods Appl. Mech. Engrg. (193) (2004) 601–629.
[29] G. Rebel, K.C. Park, C.A. Felippa, A contact formulation based on localized Lagrange multipliers: formulation and application to two-dimensional problems, Int. J. Numer. Methods Engrg. 54 (2) (2002) 263–297.
[30] J.C. Simó, T.A. Laursen, An augmented lagragian treatment of contact problems involving friction, Comput. Struct. 42 (1992) 97–116.
[31] J.C. Simó, P. Wriggers, R.L. Taylor, A perturbed Lagrangian formulation for the finite element solution of contact problems, Comput. Methods Appl. Mech. Engrg. (50) (1985) 163–180.
[32] R.L. Taylor, P. Papadopoulos, On a patch test for contact problems in two dimensions, in: W.W. Wriggers (Ed.), Nonlinear Computational Mechanics, Springer, Berlin, 1991, pp. 690–702.
[33] B.I. Wohlmuth, A mortar finite element method using dual spaces for the Lagrange multiplier, SIAM J. Numer. Anal. (38) (2000) 989–1012.
[34] P. Wriggers, Computational Contact Mechanics, Wiley, 2002.
[35] O.C. Zienkiewicz, D.W. Kelly, P. Bettes, The coupling of the finite element method and boundary solution procedures, Int. J. Numer. Methods Engrg. (11) (1977) 355–375.
[36] O.C. Zienkiewicz, D.W. Kelly, P. Bettes, Energy methods in finite element analysis, Chapter Marriage a la mode, the best of both worlds (finite elements and boundary integrals), John Wiley and Son, 1979, pp. 81–106.
[37] O.C. Zienkiewicz, R.L. Taylor, The Finite Element Method for Solid and Structural Mechanics, sixth ed., Elsevier, 2005.